ORIGINAL ARTICLE



A new procedure to derive typological fragility functions for unreinforced masonry structures: an application to a Chilean case

Juan Pablo Muñoz Gálvez¹ D· Dina D'Ayala² D· Nuria Chiara Palazzi^{1,3} D· Juan Carlos de la Llera^{1,4} D

Received: 6 March 2025 / Accepted: 13 May 2025 / Published online: 24 July 2025 © The Author(s) 2025

Abstract

The assessment of the seismic fragility of unreinforced Masonry (URM) buildings in cities, using advanced numerical approaches, is hampered by the complex connectivity which develops with the diachronic process of urban growth and regeneration. The building stock forming 43 urban aggregates in the historic neighborhood of Yungay in Santiago, Chile, is the focus of this manuscript. The Failure Mechanism Identification and Vulnerability Evaluation method (FaMIVE), a mechanical approach based on limit-state analysis and failure modes, determines the collapse load factors and derive capacity curves for each of the 423 structures surveyed and analyzed. The objective of the study is to correlate specific sets of architectural features of these buildings to their seismic performance as represented through fragility functions. To this end we have introduced a new selection algorithm to automatically group the buildings using an optimal logic tree analysis (LTA). As a result, we obtain clusters of capacity curves using the observable properties of the façades as the decision variables of the LTA, while minimizing the variability of the parameters which define the capacity curves. The median capacity curve of each cluster is then used to derive Analytical Fragility Functions (AFFs), using a capacity-demand approach, which considers different sets of nonlinear spectra. The structure of the LTA is observed to be adequately preserved for fragility functions, fully justifying the subdivision in clusters. The aim of this work is to provide the data to prioritize mitigation strategies that enables us to preserve this heritage, as well as that of other similar historical urban areas in Chile and Latin American cities, which bear a strong architectural resemblance since their foundation.

Keywords Typological fragility functions \cdot Heritage building \cdot Unreinforced masonry \cdot Aggregate structures \cdot Façade \cdot Logic tree \cdot FaMIVE



Extended author information available on the last page of the article

1 Introduction

1.1 General context

The historical densification of city centers without consistent planning has led to masonry aggregates with complex seismic interactions that are not yet fully understood. Different case studies from seismic-prone regions have shown that buildings within aggregates can exhibit better seismic performance when considered as part of a group rather than as standalone structures. However, this improved performance is not uniform across all buildings within the aggregate, with those located at the ends of rows or at corners typically being more vulnerable due to their exposure to greater seismic forces (Valente et al 2019; Leggieri et al 2021). Recent earthquakes, such as those in Italy, Portugal, Peru and Chile have exposed challenges such as separation and pounding between adjacent buildings, emphasizing the need for accurate models that account for these dynamics (Carocci 2012; Da Porto et al 2013; Palazzi et al. 2023; Putrino and D'Ayala 2019a). For example, after the 2010 Maule earthquake, the masonry aggregates of the Yungay quarter in Santiago, Chile, have revealed recurring damage patterns in URM buildings, highlighting structural vulnerabilities such as the overturning of upper wall segments (38% of cases) due to insufficient anchorage between roof trusses and main façades, as well as frequent failures in corner façades (18% overall, 62.9% in corner buildings), reflecting inadequate interlocking among orthogonal walls and lack of structural quoins. Additional issues, including partial and total façade collapse (27%) and shear-induced diagonal cracking (observed in 18–24% of cases), further emphasize the need for urban adaptation to mitigate these vulnerabilities (Palazzi et al. 2023; Putrino and D'Ayala 2019a; D'Ayala and Speranza 2003; Maio et al. 2016).

While different approaches may be used to study this kind of structures, such as the application of vulnerability indices tailored for masonry aggregates to estimate the potential damage during an earthquake (Benedetti & Petrini 1984; Maio et al. 2015), or the numerical macro-elements approach, which has been extensively used to study individual structural units within an aggregate (Lagomarsino et al. 2013; Grillanda et al. 2020; Cardinali et al. 2022), some of them overlook critical aspects such as the type of connections between adjacent buildings, the distribution of structural mass, and the irregularities in building heights and construction techniques (Lagomarsino and Giovinazzi 2006; Greco et al. 2020; Angiolilli et al. 2021). These factors result in complex dynamic interactions, influencing the overall seismic response of the aggregate (Paquette and Bruneau 2006; Lourenço et al. 2011; Betti et al. 2014), and should not be ignored. Recent research has also explored the use of advanced numerical strategies, such as non-linear dynamic analyses, to better understand the seismic response of historical masonry aggregates. These studies highlight the need for integrating large-scale vulnerability assessments with detailed local analyses to develop comprehensive seismic risk mitigation strategies for historical urban centers (Grillanda et al. 2020; Schiavoni et al. 2023; Tomić et al. 2021; Vanin et al. 2020; Bertolesi et al. 2018).

Overall, current approaches underscore the necessity of a holistic analysis that considers the interactions between masonry buildings within an aggregate, as well as the unique characteristics of each structure, to accurately assess and mitigate seismic risk (Formisano and Ademovic 2022). A suitable tool to conduct the assessment of seismic risk for these buildings in historic aggregates are analytical fragility functions, which describe the probability of a structure exceeding specific damage states under a given seismic intensity, based



on their structural analysis. Over the years, significant advances have been made in deriving fragility functions for unreinforced masonry (URM) structures. D'Ayala (D'Ayala 2013) provides a comprehensive review of these methods, tracing their development from early post-earthquake observations by Whitman (Whitman et al. 1973) and Braga (Braga et al. 1982) who introduced Damage Probability Matrices (DPMs), to the continuous vulnerability and fragility functions proposed by different authors (Orsini 1999; Singhal and Kiremidjian 2004; Rota et al. 2006; Martinelli et al. 2008; Rossetto et al. 2014).

Fragility functions may be obtained through diverse methodologies (D'Ayala 2013), namely, (a) empirical (e.g., Rota et al. 2006; Colombi et al. 2008); (b) expert judgment based (e.g., Lagomarsino and Giovinazzi 2006); (c) analytical (e.g., Kircher et al. 1997; Restrepo-Vélez and Magenes 2004; Novelli et al. 2015; Kalkbrenner et al. 2019), and (d) hybrid combination between analytical and empirical (e.g., Singhal and Kiremidjian 1998; Basaglia et al. 2018), or between expert judgment based and empirical (Jaiswal et al. 2011). The Global Earthquake Model (GEM) project provides guidelines to select the most appropriate methodology for seismic vulnerability evaluation, considering factors such as size of sample, quality of data available, and objectives and expected results (D'Ayala et al. 2015). Empirical approaches are particularly useful for large-scale studies to simulate damage scenarios, whereas analytical models are better suited for detailed assessments of individual buildings within an urban centre, but might be impractical for entire historic centres due to the considerable data acquisition and computational resources required. Despite these efforts, selecting the most appropriate fragility function for a specific building stock remains a complex task due to the heterogeneity of existing URM buildings. Researchers (Da Porto et al. 2013; Maio et al. 2015; D'Ayala 2013; Rapone et al. 2018; Maio et al. 2018; Brando et al. 2017; Ferreira et al. 2013) have addressed this challenge by developing index-based methodologies, which generate representative fragility functions for "homogeneous" building types grouped into specific classes. This classification is typically based on masonry type, which, although useful, fails to capture the considerable variability within a building stock due to other factors. Significant efforts have also been made to obtain typological fragility functions of unreinforced masonry buildings using equivalent-frame modeling (Tosto et al. 2025; Ruggieri et al. 2023). Although these studies successfully consider morphological, architectural and geometrical features for large scale analysis of historical centres—such as urban block shape, façade opening typologies, or number of storeys— additional features and local mechanisms may be considered to improve typological fragility functions. Moreover, the considered typologies are not directly transferable to other contexts such as the Chilean historic urban centres, due to differences from the urban scale to the masonry unit.

1.2 Proposed methodology

Within this context, the present research introduces a novel methodology to derive typological fragility functions for URM buildings, through a detailed case study of the historic urban Yungay quarter in central Chile, which is described in Sect. 2.1. A representative sample of URM buildings was selected for this study, as explained in Sect. 2.2, and data was collected for considered façades as detailed in Sect. 2.3. Collected data was obtained from documentation review, field work, and laboratory tests, and included architectural, geometrical and mechanical properties. Once data was collected in standardized survey forms, curated



and further systematized, the Failure Mechanism Identification and Vulnerability Evaluation (FaMIVE) method, originally developed by D'Ayala & Speranza (2003), was used to study the URM façades. The proposed approach starts by analyzing different possible collapse mechanisms—in-plane, out-of-plane, and combined—for each façade (Sect. 3.1). The acceleration that induces loss of vertical equilibrium is computed for each mechanism, and the controlling one is identified as the one with the lowest acceleration that involves the most mass. A capacity curve is then obtained for the controlling mechanism of each façade by studying an Equivalent Nonlinear Single Degree of Freedom Oscillator. Obtained capacity curves are then classified (Sect. 3.2) into different typologies based on observable properties of the façades—architectural style, geometry, materials, roof type, among others—following a novel Logic Tree Analysis (LTA) that aims to minimize the internal variability of the clusters, and produce a representative capacity curve for each façade typology. These are then (Section 3.3) used to derive analytical fragility functions using the N2 method (Fajfar and Dolšek 2012). Results are discussed and conclusions are presented in Sect. 4.

While there are existing methodologies that would allow us to classify the capacity curves (Bhattacharjee and Mitra 2021; Ran et al. 2023; Ikotun et al. 2023; Maimon and Rokach 2005), they are not adequate for our purposes, because only a single set of variables is used to characterize each façade, i.e., the parameters of its capacity curve. Any classification that relies solely on this will produce typologies that are not easy to interpret, or that fail to capture the intrinsic variability of each cluster, as will be explained in Section 3. Instead, the proposed approach characterizes each façade using two sets of variables, namely, the parameters of its capacity curve, and its observable architectural properties. While the former is used to quantify the quality of the classification, the decision variables of the logic tree correspond to the latter. The use of this second set of variables produces typologies that correctly capture the variability of each group, and that are interpretable and easy to use, since a researcher can select the most appropriate fragility function for a URM façade using only information obtained through visual inspection.

2 The Yungay quarter

2.1 General description of the Yungay quarter

The Yungay quarter, located in the north-west sector of Santiago, Chile, is one of the most representative historical areas of the centre of the capital, as recognized by a series of Supreme Decrees (Decree No 217 2000; Decree No 43 2009; Decree No 13 2019) by the *Consejo de Monumentos Nacionales* (National Monuments Council) through the Chilean Monument Law N°17.288 (Fig. 1), which eventually sanctioned it as a *Zona Tipica* (equivalent to Conservation Area), following a campaign sustained by the residents against plans for redevelopment by the municipal government (Palazzi et al. 2024). The President José Joaquín Prieto (1831–1841) founded this neighborhood on January 20, 1839, to commemorate the triumph of the Yungay battle of the War of the Confederations between Chile and Perú-Bolivia. Between 1836 and 1873, the new quarter was structured in a checkerboard pattern and designed by engineers Jacinto Cueto and Juan de la Cruz Sotomayor.

In the middle of twentieth century, the Yungay quarter underwent a substantial increase in population, which combined with lack of investment, and the damage caused by the



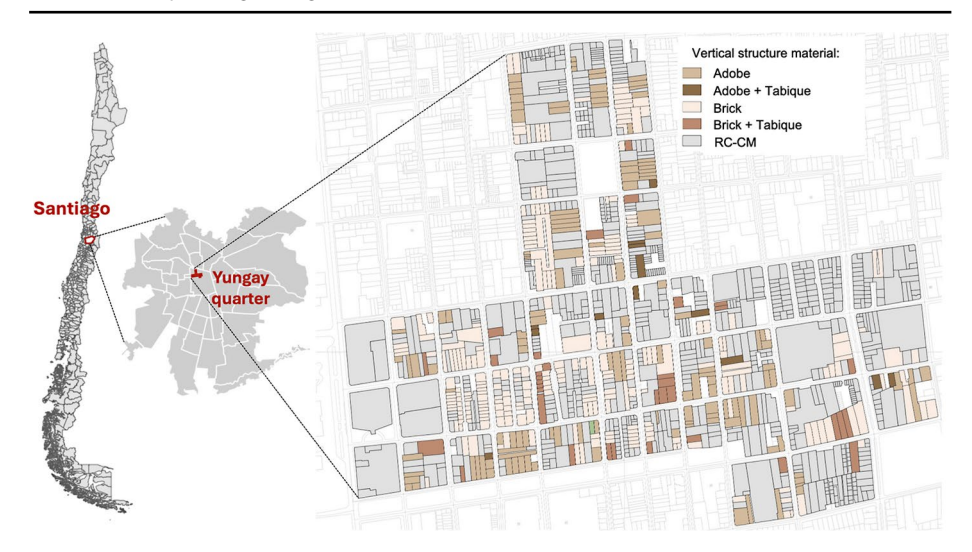


Fig. 1 Location of Yungay quarter: (a) Chile and Metropolitan region, RM; (b) 43 urban blocks of Yungay Zona Tipica (Decree No 43 2009; Palazzi et al. 2022)

Algarrobo (March 3, 1985, MW 8.0) and Maule (February 27, 2010, MW 8.8) earthquakes, led to the substantial deterioration of its built heritage. A generalized call for demolition of these historical structures damaged by seismic events was the immediate reaction from the Governmental Authority of the Santiago Metropolitan Area after the 2010 seismic event (D'Ayala and Benzoni 2012), partially stemmed by the protection status. Notwithstanding, several damaged historical buildings were replaced by new reinforced concrete and confined masonry structures four to five-stories high, causing a substantial loss of the urban heritage fabric.

Moreover, due to the constant growth and reuse of this urban area, from the Spanish colonization up to modern days, the Yungay neighborhood is now composed by heterogeneous aggregates of buildings with varied architectural, constructive, and structural properties over a territorial extension of more than 370 hectares, housing more than 58.000 inhabitants (Palazzi et al. 2023).

2.2 Selection of a representative sample

The *Zona Tipica* of Yungay quarter (Decree No 217 2000) includes 43 urban blocks and 542 historic buildings, as shown in Fig. 1. To evaluate their seismic fragility, the selection of representative stock used to estimate the vulnerability of the present case study was carried out considering the following selection criteria: (i) Type of urban blocks and lots; and (ii) Level of alteration of urban blocks with respect to the original block shape.

According to the morphological properties of the urban area (in detail analyzed in Palazzi et al. (2022, 2023), four types of urban blocks are identified, as shown in Figs. 2 and 3:

The closed block [C] is a traditional urban model of the foundational city with façades
contiguously arranged on four streets. In the Zona Tipica there are 29 [C] blocks (Fig. 3),
characterized by heterogeneous sets of structural units (SUs), generally built at different





Fig. 2 Closed (left), penetrated (center), and divided (right) blocks

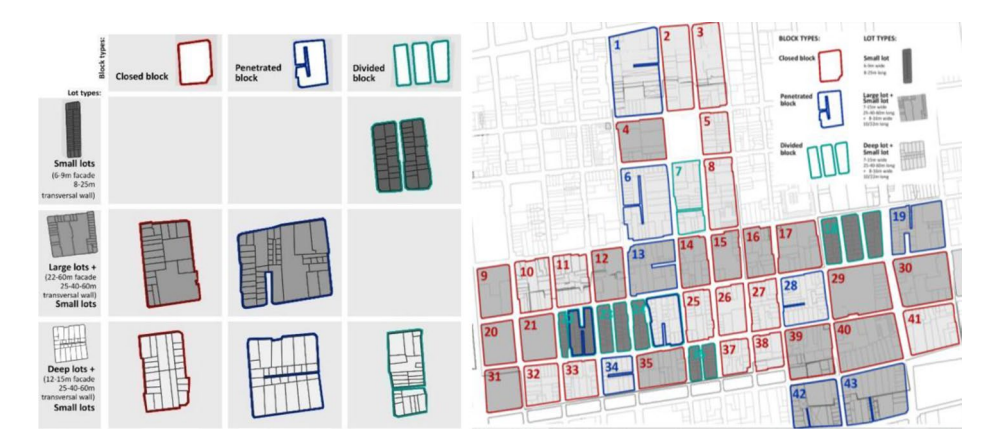


Fig. 3 Yungay *Zona Tipica*: (a) matrix of urban block typologies (closed, divided, penetrated, and mixed) vs. lot types (small lots with façade's length of 8–9 m and plot depth of 8–25 m; large lots with façade's length 22–60 m and plot depth of 25–40-60 m; and deep lots with façade's length of 12–15 m and plot depths of 25, 40, 60 m); (b) map of urban blocks and lot types

times with or without continuity of fabric and connections between buildings, in elongated rectangular-shape. Adjacent SUs are interconnected with more or less structurally effective connections, depending on their evolutionary process.

- The penetrated blocks [P] originate from an alteration of closed blocks due to the introduction of Cités at the beginning of the 20th century. The Cités are groups of aggregate dwellings which occupy and fragment a single deep lot with several social housing organized around one central or lateral alley (from 1.5 m to 6 m wide). Currently 8 penetrated blocks and 10 Cités are present in the Yungay Zona Tipica (Fig. 3).
- The divided blocks [D] consist of a closed block's decomposition by means of one or two secondary streets, into two or three separated blocks. In Yungay 4 divided blocks can be identified (Fig. 3). While the older blocks are generally constructed with unreinforced brick masonry, the newly divided urban blocks have been entirely rebuilt using confined masonry.
- Finally, two mixed penetrated-divided [-] blocks are identified (Fig. 3). These blocks, notable for their architectural significance, were among the first in Yungay to be declared part of the Zona Tipica through the Decree 217 (Consejo de Monumentos Nacionales 2000).



Throughout their evolution, the urban blocks of Yungay have undergone significant transformations associated with urban growth, including internal remodeling, vertical expansions (e.g., additions of new stories), and partial or complete reconstructions. These interventions have introduced structural discontinuities that compromise the original integrity of the aggregated building fabric. Such alterations have direct implications for the seismic performance of these structures, increasing the likelihood of out-of-plane failure mechanisms in facade macro-elements, primarily due to the weakening or absence of effective connections between adjacent wall segments. To account for these transformations, the blocks were classified into three levels of alteration, expressed as a percentage and calculated by comparing the modified built surface area (in square meters)—that is, the sum of lots that have been demolished, reconstructed, or that have undergone major structural modifications (such as the addition of new stories or the replacement of load-bearing walls or facades)—to the total surface area (in m²) of the original compact block, historically composed of simple unreinforced masonry units. The thresholds are defined as follows: (i) low alteration: less than 30% of the block's built surface modified; (ii) medium alteration: between 30% and 70%; and (iii) high alteration: more than 70%.

Using these criteria, 21 blocks were selected as a representative sample from the 43 blocks that make up the Yungay quarter. As detailed in Table 1, the sample reflects a balanced distribution across the four block typologies and different lot dimensions. Blocks with low levels of alteration are generally associated with deep plots, while the majority of the selected blocks present medium levels of alteration.

2.3 Data collection and adaptation of the FaMIVE procedure

A detailed inspection and data collection survey was then carried out in the period January to April 2023, for 423 historical façades, by a team of three conservation architects and two engineers, who were trained to collect the data according to the form for the Failure Mechanism Identification and Vulnerability Evaluation (FaMIVE) method (Guardiola Villora et al. 2024). The objective of the onsite survey phase is to record parameters useful to determine the seismic vulnerability of these façades and to document their post-earthquake damage, where this is still visible. The survey is organized to: i) first define the adjacence

Divided UBs Closed UBs Penetreted UBs Mixed UBs (Total: 30) (Total: 8) (Total: 3) (Total: 2) <30% 25, 11 6,34 7 Urban ≥30% blocks % of and ≤ 12, 36 2, 33 13, 42 1,28 36 22, 24 alteration 70% 23 ≥70% 4, 16 19, 43

Table 1 Indexes of the urban blocks selected for the FaMIVE analysis, according to Fig. 3



and connection of each building to the neighboring ones, then ii) to dissect each building in Macro-Elements (façade, walls, horizontal structures and roof) and determine their typologies; iii) to collect the geometry of each Macro-Element including layout of openings and connections with other macroelements; iv) presence of additional restraining elements which may alter the structural response; v) classification of load bearing structures, along with the average size of the units that compose the Macro-Element; vi) classification of additional vulnerability elements; and vii) identification and description of damage record and crack pattern (if present). The data are collected, stored and processed by means of an electronic application developed in Visual Basic and embedded in Excel ® elaborated by the authors in previous work (D'Ayala 2013) and adapted specifically to the heritage structures of the Barrio Yungay (Palazzi et al. 2022, 2024).

In order to adapt the FaMIVE procedure to the peculiarities of the Chilean heritage buildings and understand their homogeneity and differences, which affect their seismic response, a set of parameters, describing architectural features, geometrical parameters and mechanical properties, are summarized in Table 2, and illustrated in Figs. 4, 5, 6, 7, 8. These properties are then used to develop the decision algorithm of the logic tree, cluster the capacity curves and derive the fragility functions as further discussed in Sect. 3. The properties considered are: (i) architectural style (Colonial derivation [CD] in Figure 4a, and Classicist [CL] in Figure 4b); (ii) wall materials (brick masonry [B] in Fig. 5 or adobe [A] masonry in Fig. 6); (iii) floor types (direction of wooden beams located parallel [P] or orthogonal [O] to main façade, or presence of slab [S]); (iv) number of good connections to orthogonal walls (0, 1 or 2); (v) number of stories (1, 2 or 3 stories); (vi) roof types (heavy or light trusses mono-pitch type 1, or 2, slab in Fig. 7 and Table 2); and (vii) the presence of vertical addictions (*antetecho* of adobe masonry [AA] in Fig. 8a-b, brick masonry [AB] in Fig. 8c, wooden [AW] in Fig. 8d, tympanum [TT] in Fig. 8e, and without vertical addiction [00] in Fig. 8f).

Geometrical parameters—such as total façade height, wall thickness at the first floor, effective area and length, average number and size of openings, among others—were obtained through direct field surveys of the Yungay buildings, by means of in-situ measurements, visual inspections, and photographic documentation. The characterization of masonry mechanical properties was carried out through material testing on two representative specimens, each corresponding to one of the most recurrent brick masonry types identified in the study area. The tests included compression tests on bricks and mortar, tensile strength tests on masonry cores, and cohesion coefficient measurements between bricks and mortar. Specifically, specimens were extracted from a structure built in Masonry Type B1 (1-leaf brickwork), and tested for compression, tensile strength, and cohesion; a second set of specimens corresponding to Masonry Type B2 (2-leaf brickwork) were tested for compression and brick-mortar cohesion. Regarding adobe masonry, direct material testing was not feasible within the scope of this study. Therefore, the mechanical parameters adopted for these typologies were based on the Chilean national standard NCh3332:2013 – Structural design - Retrofitting of historic earth buildings - Requirements for the structural design planning NCh3332:2013 (2013), which provides reference values for earthen construction commonly found in heritage buildings, while some additional values were obtained from other sources (Ministerio de Vivienda 2017; Gonzales and Edwards 2016). More details of the results of the mechanical tests and considered mechanical parameters are presented in Annex A.



Table 2 Categorization of architectural features and their statistical distribution among Yungay historic buildings obtained by direct observation, sorted by type (categorical—C, integer number—I, and real number—R)

Parameter	Symbol	Туре	Possible values / range and [unit]	ID	Number of façades per category		
Architectural	A _{sty}	С	Colonial derivation	CD	253 170		
style			Classicist and variant	CL	6 9		
			Truss-Light Mono-pitch type 1	2L0 1L1	178 121 72 43 9		
Roof type	R _{typ}	С	Mono-pitch type 2 Truss-Heavy	1L2 2H0	2L0 - 1L1 - 1L2 - 2H0 - 2H0 - 3		
			Slab	<i>S</i> 00			
	l		1-leaf brickwork 1-leaf adobe work	B1 E1	119		
Masonry type	M _{typ}	С	2-leaf Brickwork	B2	17 17 13 14 1 18 18 18 18		
			2-leaf adobe work 3-leaf brickwork	E2 B3			
			No addition	00	270		
Vertical	Vadd	c	Wood antetecho Brick antetecho	AW AB	63 41 26 23		
additions	uuu		Adobe antetecho	AA	00 A A F + + + + + + + + + + + + + + + + +		
			Tympanum Main bearing	TT			
			elements orthogonal to façade	0	401		
Floor type	F _{typ}	С	Main bearing elements parallel to	P	19 3		
			façade		0 4 S		
			Slab Brick	S	278		
Material of first	m_{fs}	С	Adobe	A	145		
story	,		Adobe	A	В - Ч		
Presence of	Q	c	True / False		351 72		
quincha	`				1 0		
Number of good					288		
connections to orthogonal	N _{con}		{0,1,2} [-]	-	43 92		
walls					0 1 2		
Number of	,,	,	{1,2,3} [-]		119		
stories	N _{sto}	'	{1,2,3}[-]	-	1 2 3		
					139 166		
Total height	H _{tot}	R	[3.01, 13.00] [m]	-	54 42 22		
					3 5 7 9 11 13		
Total length	,	R	[2.40, 31.04] [m]		75 5 3		
rotar length	L _{tot}	"	[2.40, 31.04] [111]	-	2 8 14 20 26 32		
					224 139		
Effective area	A_{eff}	R	[0.44, 0.97] [-]	-	3 57		
					0.40 0.55 0.70 0.85 1.00		
Fff and the feet of	,		[0.25.4.00] F.3		56 126		
Effective length	Leff	R	[0.25, 1.00] [-]		0.25 0.50 0.75 1.00		
Average					175		
number of openings per	\bar{O}_N	R	[1.00, 6.00] [-]	-	52 43 87 66		
story					1 2 3 4 5 6		
Average	-		fo.oo a.co.; ;		102		
opening width	\bar{O}_w	R	[0.00, 3.00] [m]	-	0.8 1.5 2.0 2.5 3.0		
					267		
Average opening height	\bar{O}_h	R	[0, 3.88] [m]	-	51 100 5		
					1 2 3 4 5		
Wall thickness	t _{bot}	R	[0.21, 1.00] [m]		76 94 18		
at bottom	- 500		,,		0.2 0.4 0.6 0.8 1.0		
	1	1	1	1 1	ı		





Fig. 4 Architectural style Palazzi et al. (2022): (a) Colonial Derivation style (CD), and (b) Classicist & Variant (CL&Va)

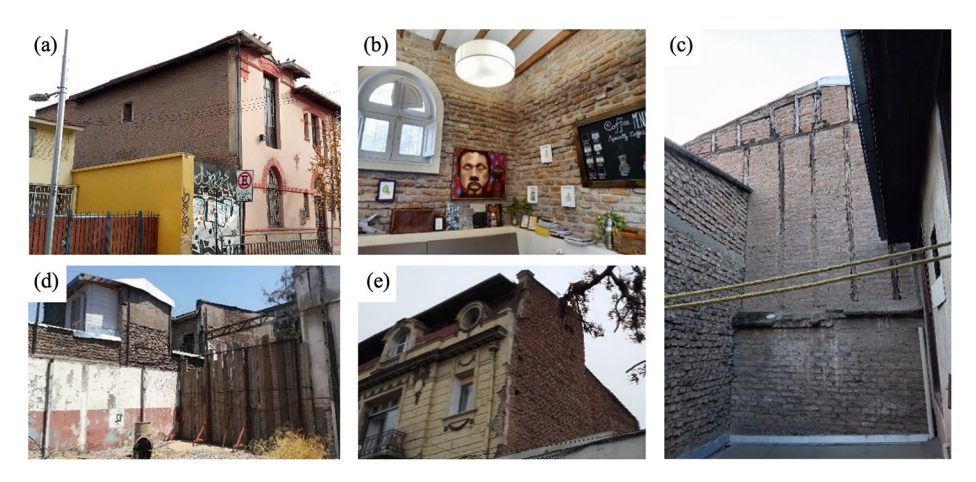


Fig. 5 Brick masonry types in Barrio Yungay



Fig. 6 Adobe masonry types in Barrio Yungay





Fig. 7 Roof types: (a, b) timber trusses, (c, d, e) timber mono-pitch

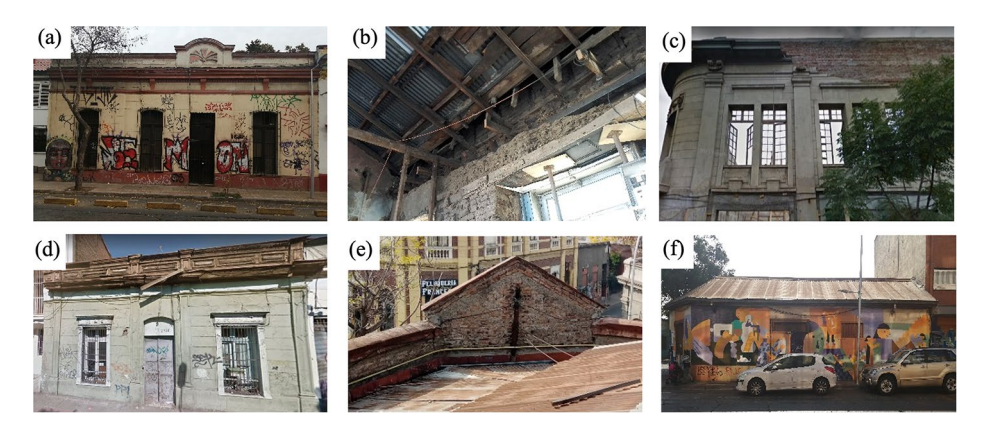


Fig. 8 Vertical additions: (a, b) adobe antetecho [AA]; (c) brick antetechos [AB]; (d) wooden antetecho [AW]; (e) brick tympanum [TT]; and (f) without antetecho [00]

3 A new procedure to derive typological fragility functions for URM structures

With the aim of obtaining seismic fragility functions for a large number of historical buildings, in this research the well-known analytical method, FaMIVE (D'Ayala 2005), is applied. The procedure is based on limit analysis and failure modes (in-plane, out-of-plane and combined collapse mechanisms) to derive capacity curves. Once the capacity curves are obtained for the complete stock of façades (423), a new algorithm is proposed to automatically classify them in an optimal logic tree, obtaining a representative capacity curve for each cluster. Then, the capacity curve of each cluster is used to obtain representative fragility functions using a capacity-demand approach, with a consistent set of Chilean seismic strong motion records. The new procedure is presented step-by-step in the following sections.



3.1 Failure mechanism identification and vulnerability evaluation analysis (FaMIVE)

The FaMIVE method has been applied to estimate the seismic fragility and vulnerability of masonry buildings in arrays and aggregates in different locations worldwide, from Italy (D'Ayala and Speranza 2003; D'Ayala and Paganoni 2011; Putrino and D'Ayala 2019b), to Nepal, India (D'Ayala and Kansal 2004), Turkey (D'Ayala and Yeomans 2004), Slovenia (Bosiljkov et al. 2015), Algeria (Novelli et al. 2015) and more recently Spain (Guardiola-Villora et al. 2023). This analytical approach, based on limit state analysis of URM structures, correlates collapse load factors and collapse mechanisms to specific constructional properties of the external bearing walls and façades. FaMIVE allows to compute load multipliers, λ , for horizontal equivalent forces that produce the activation of different collapse mechanisms of the URM macro elements under analysis, given their geometrical and structural properties, as well as their constraints. Assuming that the masonry comply with a Mohr-Coulomb failure criterion, characterized by cohesion strength, friction coefficient and bounded compressive strength, the overturning collapse load multiplier $\lambda_{(O),j}$, is obtained through Eq. 1.

$$\lambda_{(O),j} = \frac{\sum_{i=1}^{j} \frac{T_{i}^{2}}{2} L + \left(\varepsilon + \beta\right) \frac{h_{s}}{2} j^{2} \tan \alpha_{j} T_{s} \left(\frac{h_{s}}{3} \tan \alpha_{j} + T_{i}\right) + kL \left[\frac{T_{N}}{2} + \mu h_{s} j + \sum_{i=1}^{j} \cdot \left(T_{i} + \Delta T + \mu h_{s} \left(j - i\right)\right)\right]}{h_{s} \left[\sum_{i=1}^{j} L T_{i} \left(j - i + \frac{1}{2}\right) + \left(\varepsilon + \beta\right) \frac{h_{s}^{2}}{3} j^{3} \tan \alpha_{j} T_{s} + kL \left(j + \sum_{i=1}^{j} \left(j - i\right)\right)\right]}$$

In Eq 1, which is based on a lower bound approach of the limit state analysis, T_i is the thickness of the façade at each storey, T_s the thickness at the storey affected by the hinge, and T_N the thickness at the top of the wall, L is the width of the façade participating to the mechanism, j is the number of stories involved and the story level at which the hinge is positioned; h_s the story height, α_j is the inclination of the crack on the vertical in the party walls, μ is the coefficient of friction. The numerator computes the stabilising forces including the positive effect of friction on the restraining actions of the floors on the walls, and the denominator sums up the overturning forces generated by lateral acceleration, including the floor masses; $\lambda_{(O),j}$ is therefore directly expressed in terms of gravity acceleration, while the masses of walls and floors are normalized by considering a factor k which provides the ratio of the unit volume weight of the floor structures to the masonry structures. The coefficients ε and β account for the presence/absence of internal bearing walls and party walls, respectively, connected to the macro elements in reason of the masonry fabric and bond layout, so that the constraints conditions for the overturning are fully determined.

Equation 1 can then be customised to represent 8 different possible collapse mechanisms by varying the terms at the numerator and denominator to represent the geometry and mechanics of the collapsing portions including the contribution of orthogonal walls or other restraints. Using the same approach, a set of equations can also be developed for in plane mechanisms considering the possible failure of both piers and spandrels, leading to a set of $\lambda_{(D,j)}$ collapse load factors (Novelli et al. 2015), therefore providing a full gamut of possible failure modes. For more details the reader is referred to D'Ayala and Speranza (2003). The assumption is that among all of them, the one yielding the lower value of λ , while also maximizing the volume of macro-element mobilized, including floor and roof structures, is the one most critical for the considered building. So called local mechanisms



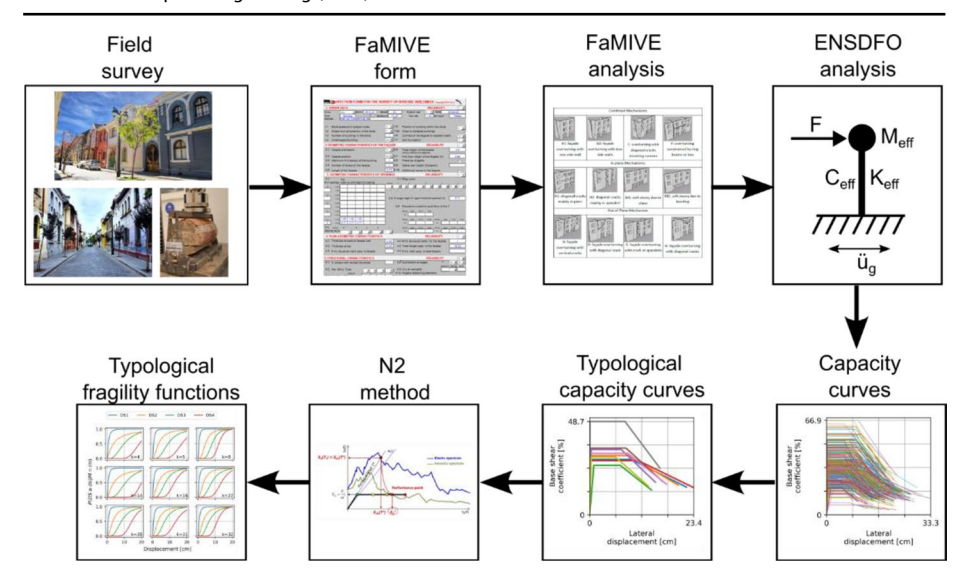


Fig. 9 Steps of FaMIVE methodology. N2 method figure from D'Ayala (2015)

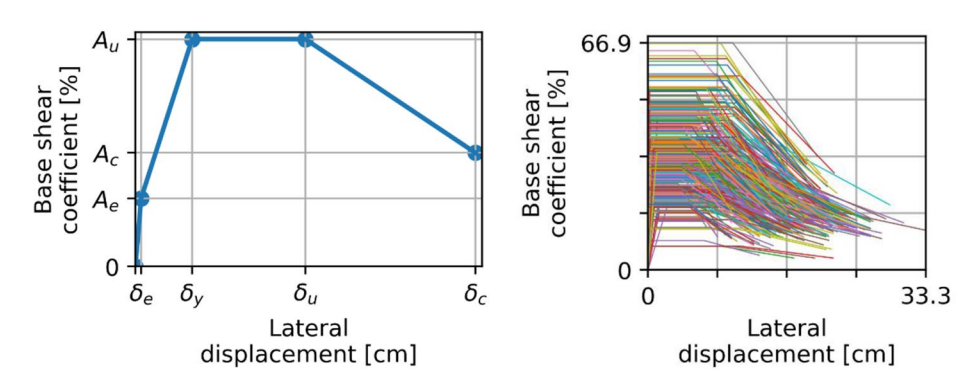


Fig. 10 (a) General form of a capacity curve; and (b) Capacity curves obtained for the façades of the Yungay quarter using the FaMIVE methodology

are included by considering the occurrence of partial mechanisms at each storey, for gables or other features of the façade.

This generic set of equations can be customised to accommodate all geometric and constructional details of the various typologies identified in the building stock under analysis, by using a data collection form (Guardiola Villora et al. 2024) (Fig. 9), tailored to capture such details and incorporating them in the computational Visual Basic platform.

The different steps of the FaMIVE methodology are presented schematically in Fig. 9, while the capacity curves obtained for the façades of the Yungay quarter are presented in Fig. 10b. These capacity curves are then automatically classified through a new algorithm that uses an optimal logic tree analysis (LTA), as explained in the next section.

To develop a fully integrated performance based probabilistic risk assessment, for each analyzed macro-element, a capacity curve is derived using an Equivalent Nonlinear Single



Degree of Freedom Oscillator (ENSDFO) to determine the drift at which any of four damage thresholds are reached. The derivation of the four-linear capacity curve (see Fig. 10a) and the computation of the damage thresholds is discussed in detail elsewhere (D'Ayala 2013). These create four possible damage states: damage limitation (DL) corresponding to the elastic limit capacity associated to the attainment of the tensile strength at the cracked cross-section, significant damage (SD) corresponding to the first peak force capacity point, extensive damage (ED) represented by the maximum displacement at maximum force capacity, and the collapse (C) limit state corresponding to the 50% loss of force capacity for increasing displacement. The greater reliability of the FaMIVE procedure in respect to other mechanism approaches, is related to the preserved fidelity of the capacity curves of the ENSDOF model and the selected damage thresholds to each macro element analyzed, by allowing the retention of a high level of detail of the geometry and kinematics of the problem. At the same time, since only the ultimate conditions are computed, FaMIVE does not require the computational resources, or time demands of a typical nonlinear pushover analysis. The full sample considered in this study can be analyzed on an Intel i7 configuration laptop in about 90 minutes. Therefore, sensitivity analysis for a variety of parameters is also possible, within a very reasonable amount of time. The idealized shape of a capacity curve is represented in Fig. 10a, while the set of capacity curves obtained is presented in Fig. 10b. A capacity curve is defined by acceleration values at first crack (A_e) , plateau (A_u) , and collapse (A_c) , as well as their associated deformation levels at first crack (δ_e) , beginning and end of the acceleration plateau (δ_y and δ_u , respectively), and collapse (δ_c).

To determine the performance points the N2 method is implemented (Fajfar and Gašperšič 1996), whereby for each capacity curve representative of an analyzed Macro Element, its intersection with the corresponding nonlinear spectrum is identified, hence also accounting for the available ductility of the system. The N2 method can be implemented using various representations of the earthquake spectra depending on the purpose of the study, from idealized design spectrum, to set of natural spectra consistent with the local seismicity or generic catalogues of spectra. However the interest in this study is not to determine the performance of a specific building, in order to decide on a specific strengthening design, but to develop a tool which allows the development of fragility functions which can be directly correlated to specific architectural and construction feature, so that, once available can be applied to a much larger set of the building stock than the one analyzed here, in support of conservation and retrofitting strategies at urban, district and national level, allowing to maximize the benefit from investment and minimize the disturbance to the heritage character. Therefore, in the next section we provide a novel approach to create homogeneous groups of buildings within the analysed sample, with the objective of obtaining a reduced number of representative capacity curves then used to derive the fragility functions.

3.2 Building clustering and logic tree analysis (LTA)

It may be appreciated in Fig. 10b that the capacity curves of the Yungay quarter show important variability, both in terms of strength and displacement capacity. For instance, the base shear varies between 10% and 65% of the total weight, while the maximum displacement at collapse take values between 7 and 35 cm. This is also reflected in the variety of collapse mechanisms computed as critical. Hence, using a single capacity curve to represent all façades would not be a good approximation. The solution proposed herein is to classify the



capacity curves into clusters, and then to define a representative capacity curve for each one. With this in mind, a methodology determining a small practical number of representative parametrized homogeneous clusters is explained next. The method aims to minimize the internal variance of the clusters and to control the outliers, so that each group is sufficiently compact, and considers properties that may be easily obtained by visual inspection (e.g., architectural style, number of stories, wall thickness) as decision variables. To formally state the problem, the i-th façade, f_i , may be represented by two variables:

$$f_i = \{c_i, p_i\}; c_i = [(A_u)_i \ (\delta_u)_i \ (\delta_c)_i]; p_i = [p_i^{(1)} \ p_i^{(2)} \ \dots \ p_i^{(N_p)}]$$
 (2)

The first variable, c_i is a vector representation of the capacity curve of the façade, where $(A_u)_i$ is the plateau acceleration, $(\delta_u)_i$ is the deformation at which the acceleration plateau ends, and $(\delta_c)_i$ is the post-yield deformation at which the acceleration reaches a value of $(A_c)_i = (A_u)_i/2$, as presented in Fig. 10a. Although additional parameters are used to completely define a capacity curve, only these three are considered for the classification process. The second variable, p_i is a list of the façade properties, where $p_i^{(j)}$ is the value of the j-th property, $j = \{1, \ldots, N_p\}$, and N_p is the total number of properties considered in this study, summarized in Table 2. Similarly, a set of façades, $\mathcal{F} = \{f_1, \ldots, f_{(N_f)}\}$ may be understood as a set of capacity curves, $C = \{c_1, \ldots, c_{N_f}\}$, with a corresponding set of façade properties, $P = \{p_1, \ldots, p_{N_f}\}$, where N_f is the number of façades. Hence, we may characterize the set \mathcal{F} as $F = \{C, P\}$, where membership of a façade to a set is exclusive.

While there are methodologies that would allow to classify the set of façades, F, in a decision tree (Bhattacharjee and Mitra 2021; Ran et al. 2023; Ikotun et al. 2023; Maimon and Rokach 2005), they are not adequate for our purposes, because these methods would use the capacity curves, C, for the classification process. This means that two different façades could go into the same group just because they are similar in terms of C, while completely ignoring their (dis)similarity in terms of P. Alternatively, façades that are similar in terms of P, and that should therefore belong to the same group, could be spread between clusters. The consequence of this is that interpretability and generalization of the results would be modest, as it would not be possible to simply perform a visual inspection of a new façade (e.g., according to a subset of the attributes of the properties P) and predict its seismic behavior (i.e., capacity curve, and therefore, its fragility function). The obtained clusters would be rather artificial and the intrinsic variability of a typology of façades would not be correctly accounted for. By enforcing the classification algorithm to use the façade properties, P, to classify their performance, it is possible to get the desired interpretable results in terms of mean and variance of the capacity curves, C, for different typologies of façades, and later in terms of their fragility functions. The second reason why the existing methods are not adequate is because they work with numerical variables, while in this case the facade properties include numerical (both continuous and integer) and categorical values at the same time. Hence, a more general approach is required.

The problem may be stated as follows: how can the initial set of façades be classified in a logic tree that makes sense in terms of the combination of properties that are present within each cluster, while guaranteeing that the proposed classification is the best possible one by a reasonable metric representing their seismic performance? This classification may be interpreted as an optimization problem, where the goal is to minimize the internal vari-



ability of all clusters of capacity curves, while using the combination of façade properties as decision variables for the logic tree. The proposed problem is rather complex given its combinatorial nature, and it may be simplified for practical uses to reduce its computational cost. Instead of simultaneously minimizing the variability of all clusters, the optimization problem may be applied incrementally, to reach a sufficiently good local optimal solution. Since the classification using a logic tree implies dividing the set of façades in smaller and smaller subsets, let us define a subset of façades as:

$$F^{(k)} = \left\{ C^{(k)}, P^{(k)}, S^{(k)} \right\} \tag{3}$$

where, $C^{(k)}$ and $P^{(k)}$ are the subsets of capacity curves and properties of the k-th cluster, respectively; $S^{(k)}$ is a variable that summarizes the properties in $P^{(k)}$, as will be defined later; $k = \{0, \ldots, N_c\}$ is the index of the cluster, with k = 0 corresponding to the initial set of façades; and N_c is the total number of clusters, other than the initial one. Therefore, $F^{(k)} \subseteq F^{(0)}$, $C^{(k)} \subseteq C^{(0)}$, and $P^{(k)} \subseteq P^{(0)}$.

The subset of capacity curves may be defined as:

$$C^{(k)} = \left\{ c_1^{(k)}, \dots, c_{N_f^{(k)}}^{(k)} \right\} = \left\{ \begin{bmatrix} (A_u)_1^{(k)} \\ (\delta_u)_1^{(k)} \\ (\delta_c)_1^{(k)} \end{bmatrix}, \dots, \begin{bmatrix} (A_u)_{N_f^{(k)}}^{(k)} \\ (\delta_u)_{N_f^{(k)}}^{(k)} \\ (\delta_c)_{N_f^{(k)}}^{(k)} \end{bmatrix} \right\}$$
(4)

where $c_i^{(k)}$ is the *i*-th capacity curve in the subset, with $i = \left\{1,\ldots,N_f^{(k)}\right\}$; $N_f^{(k)}$ is the number of façades in the *k*-th cluster; and $(A_u)_i^{(k)}$, $(\delta_u)_i^{(k)}$, and $(\delta_c)_i^{(k)}$ are the same properties of Eq. 3, but for the *i*-th façade of the *k*-th cluster.

In turn, the subset of properties may be defined as:

$$P^{(k)} = \left\{ p_1^{(k)}, \dots, p_{N_f^{(k)}}^{(k)} \right\} = \left\{ \begin{bmatrix} p_1^{(k,1)} \\ \vdots \\ p_1^{(k,N_p)} \end{bmatrix}, \dots, \begin{bmatrix} p_{N_f^{(k)}}^{(k,1)} \\ \vdots \\ p_{N_f^{(k)}}^{(k,N_p)} \end{bmatrix} \right\}$$
(5)

where $p_i^{(k)}$ is the vector of properties of the *i*-th façade of the *k*-th cluster; and $p_i^{(k,j)}$ is the *j*-th component of $p_i^{(k)}$, with $j = \{1, \dots, N_p\}$.

Finally, the summary variable of the cluster is defined as:

$$S^{(k)} = \begin{bmatrix} s^{(k,1)} \\ \dots \\ s^{(k,N_p)} \end{bmatrix}$$
 (6)

where $s^{(k,j)}$ is the set of values present in the j-th property of the k-th cluster, i.e., $p_i^{(k,j)}$.

Having defined the initial set $F^{(0)} = \{C^{(0)}, P^{(0)}, S^{(0)}\}$, the proposed classification methodology starts by dividing $F^{(0)}$ into two subgroups, $F^{(1)}$ and $F^{(2)}$, using the summary vector $S^{(0)}$, as will be explained later, so that the variances of the resulting subsets of capacity curves, $C^{(1)}$ and $C^{(2)}$, are as small as possible. Then, the same procedure is applied to



each resulting subset $F^{(k)}$, until a stop criterion is met. It is important to mention that the stop criterion is evaluated for each subset $F^{(k)}$ independently of the others, allowing the logic tree to have branches with different widths and depths. The present scheme will, at most, duplicate the number of clusters with each further level of depth of the logic tree. The exponential growth requires a standardized numbering of the subsets, as the one in Fig. 11, which also indicates the level of growth of each branch.

To explain the division logic and the stop criterion, let us consider any cluster $F^{(k)} = \{C^{(k)}, P^{(k)}, S^{(k)}\}$. The method seeks to divide it into two subgroups $F^{(m)}$ and $F^{(n)}$, where m and n are indexes consistent with the selected numbering scheme (e.g., if the order of Fig. 11 is used, k = 5 implies m = 11 and n = 12). The division of $F^{(k)}$ is carried out by selecting a single property of $S^{(k)}$, namely the d-th one, $s^{(k,j=d)}$, and subdividing its attributes or range of values into two mutually exclusive and collectively exhaustive subsets, $s_m^{(k,j=d)}$ and $s_n^{(k,j=d)}$. The façades in $F^{(k)}$ are then rearranged according to the membership of their d-th property to either subset. In this way, all the façades whose d-th property, $p_i^{(k,d)}$, is contained in the subset $s_m^{(k,j=d)}$ are assigned to the first subgroup, $F^{(m)}$, and the others are assigned to the second subgroup, $F^{(n)}$. Based on this, it is straightforward to obtain the elements of $F^{(m)}$ and $F^{(n)}$, by appending the vectors of capacity curves $(c_i^{(k)})$ in $C^{(m)}$ and $C^{(n)}$; and properties $(p_i^{(k)})$ in $P^{(m)}$ and $P^{(n)}$, as appropriate, while $S^{(m)}$ and $S^{(n)}$ may be constructed at the end of the split, by checking the values present in $P^{(m)}$ and $P^{(n)}$. Even though a single property is considered at each stage of the subdivision (i.e., d = 1), the range of attributes or values of other properties of $S^{(m)}$ and $S^{(n)}$ may also change after rearranging the facades into $S^{(m)}$ and $S^{(n)}$, if some of the properties are correlated.

It is evident that the key aspects in the construction of the logic tree are (i) the selection of the property $s^{(k,j=d)}$ used for the split; and (ii) the definition of the two mutually exclusive and collectively exhaustive subsets, $s_m^{(k,j=d)}$ and $s_n^{(k,j=d)}$. A procedure is presented next to select the optimal combination of both aspects, as well as stopping criteria to prevent further branching of the logic tree. First, the fitness of a cluster must be quantified, so it is possible to compare different divisions to select the best one. Given a cluster of façades, we may compute different statistical values for each component of $C^{(k)}$, such as:

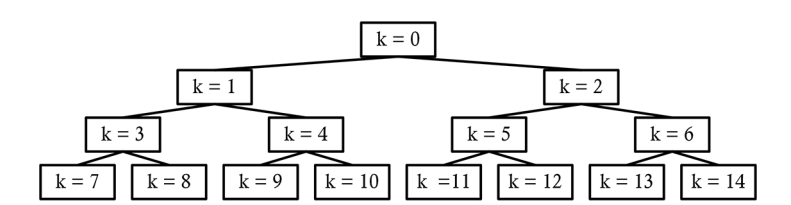


Fig. 11 Structure of the logic tree



$$\mu^{(k)} = \begin{bmatrix} mean \left[(A_u)_i^{(k)} \right] \\ mean \left[(\delta_u)_i^{(k)} \right] \\ mean \left[(\delta_c)_i^{(k)} \right] \end{bmatrix}; \sigma^{(k)} = \begin{bmatrix} std \left[(A_u)_i^{(k)} \right] \\ std \left[(\delta_c)_i^{(k)} \right] \\ std \left[(\delta_c)_i^{(k)} \right] \end{bmatrix}; v_{max}^{(k)} = \begin{bmatrix} max \left[(A_u)_i^{(k)} \right] \\ max \left[(\delta_u)_i^{(k)} \right] \\ max \left[(\delta_c)_i^{(k)} \right] \end{bmatrix}; v_{min}^{(k)} = \begin{bmatrix} min \left[(A_u)_i^{(k)} \right] \\ min \left[(\delta_u)_i^{(k)} \right] \\ min \left[(\delta_c)_i^{(k)} \right] \end{bmatrix}$$

$$(7)$$

where $\mu^{(k)}$, $\sigma^{(k)}$, $v_{max}^{(k)}$, and $v_{min}^{(k)}$ are the component-wise mean, standard deviation, maximum and minimum values of the capacity curves in $C^{(k)}$. These values may be used to compute the cluster fitness; however, the selection of the fitness function is problem dependent. Different options were evaluated for the case study, and the one that produced the best results, without losing interpretability, corresponds to:

$$h^{(k)} = w \cdot \left(max \left\{ \left| v_{max}^{(k)} - \mu^{(k)} \right|, \left| v_{min}^{(k)} - \mu^{(k)} \right| \right\} : \sigma^{(k)} \right)$$
 (8)

where $w = [w_{A_u}, w_{\delta_u}, w_{\delta_c}]$ is a weight vector that indicates the relative importance of different components of the capacity curve in measuring the fitness of the cluster and is normalized so that the sum of its components is unitary. Each of the statistical values is in fact a vector, hence, the ":" operand indicates a component-wise division, and the "." indicates a dot product, thus, $h^{(k)}$ is a scalar, corresponding to a weighted average of the component-wise maximum distance between any capacity curve in the cluster, and the mean curve of it, normalized by its standard deviation. The idea behind the selected fitness function is to avoid outliers in the resulting cluster, therefore its mean capacity curve being a more robust representation of the seismic response of the façades contained in the cluster, and to avoid skewness.

Given a set of façades $F^{(k)}$, and any division of it in subsets $F^{(m)}$ and $F^{(n)}$, we may compute the fitness of the subsets with Eq. 8 to obtain $h^{(m)}$ and $h^{(n)}$, and then define the fitness of the division as:

$$h_{m,n}^{(k)} = max \left(h^{(m)}, h^{(n)} \right)$$
 (9)

Therefore, given a group of façades, $F^{(k)}$, at any level of the logic tree, we aim to optimally divide it into two subgroups by solving the minimization problem local to that branch of the tree:

$$\min \left\{ h_{m,n}^{(k)} \left(F^{(k)}, d, \ s_m^{(k,j=d)} \right) \right\}$$
 (10)

where the decision variables are the selection of the property to be used for the split, d, and the definition of the subset $s_m^{(k,j=d)}$ (and its complement $s_n^{(k,j=d)}$). The minimization problem may also include restrictions, for example, by adding penalty factors to the fitness function. For numerical variables, both integer and real, the optimal threshold value may be obtained numerically, while for categorical variables, the optimal subgroups may be obtained by exhaustive search, or by using a metaheuristic. An optimal division may be obtained for each property, and then the best one of those is selected as the solution of the minimization problem.

Once an optimal solution has been obtained for $F^{(k)}$, the method is then applied to the resulting subgroups $F^{(m)}$ and $F^{(n)}$ recursively until a stopping criterion is met. The divi-



sion of a cluster is carried out only if (i) the fitness of the subgroup exceeds a tolerance limit F_{max} ; (ii) the subgroup contains enough elements to produce subgroups that are composed of at least N_{min} members each; and (iii) the maximum tree depth, D_{max} , has not been reached yet. The stopping criteria are evaluated for each new potential ramification of the logic tree independently, which allows to get asymmetrical trees where some branches are longer or wider than others. Additionally, since the goal at each step is to produce an optimal split, the algorithm indirectly tries to produce a logic tree with no excessive depth.

The classification algorithm was implemented in Python (Ahumada et al. 2025) and run considering a fitness tolerance of $h_{max}=1.5$, a minimum number of $N_{min}=20$ elements per group, and a maximum depth of $D_{max}=6$ levels. The selected fitness tolerance implies that the algorithm stops the branching process for any given group if the curve that deviates the most from the mean curve of the group, is located at a distance less than 1.5 standard deviations from it (on average, after applying the weights) Although the branching process could stop before reaching that threshold if the elements in a cluster do not allow for a division where each subcluster has at least N_{min} elements, or if the maximum depth is reached. The analysis was carried out considering the properties of Table 2, and a weight vector $[w_{A_u}, w_{\delta A_u}, w_{\delta_c}] = \left[\frac{1}{3}, \frac{1}{3}, \frac{1}{3}\right]$, i.e., equal importance is given to ultimate displacement, ultimate strength, and collapse displacement. These parameters are considered due to the important variability observed earlier, and because a classification of the fragility functions based on them is easy to interpret.

The obtained logic tree is presented in Fig. 12 with the properties of each cluster summarised in Table 3. The algorithm is forced to make the first division by architectural style, to ease results interpretability, therefore, the upper part of the tree corresponds to façades with architectural style "Colonial derivation" (CD), while the lower part corresponds to "Classicist and variant" façades. The initial group of façades is classified into the 13 typologies summarized in Table 3, that correspond to the end-clusters of the logic tree, although intermediate cluster may also be used. The algorithm is quite flexible, therefore different logic trees may be obtained if changes are made to the fitness function, weight vector, restrictions, or override decision for the initial splits of the tree, as will be explained in the following section. Different configurations or optimization of the hyper-parameters can be investigated using well established methodologies for this type of problems (Yang and Shami 2020). The capacity curves corresponding to each of the clusters identified are shown in Fig. 13, where solid lines are used to represent the Classicist buildings clusters, while Colonial Derivation clusters are depicted using dotted lines. It is noticeable that the first group has a greater variance with the resulting clusters capacity curves differing substantially for maximum force capacity, ultimate and collapse displacements. On the other end the capacity curves for the clusters of Colonial Derivation, notwithstanding having greater membership (257 against 170) both as a whole and in the subsets (on average 36 against 28), has a much smaller variability in terms of force capacity and ultimate displacement, with significant variance only in the collapse displacement. Please note that fitness values in Table 3 are larger than the tolerance of 1.5, because the LTA cannot further divide the cluster without obtaining new clusters with less than N_{min} elements.



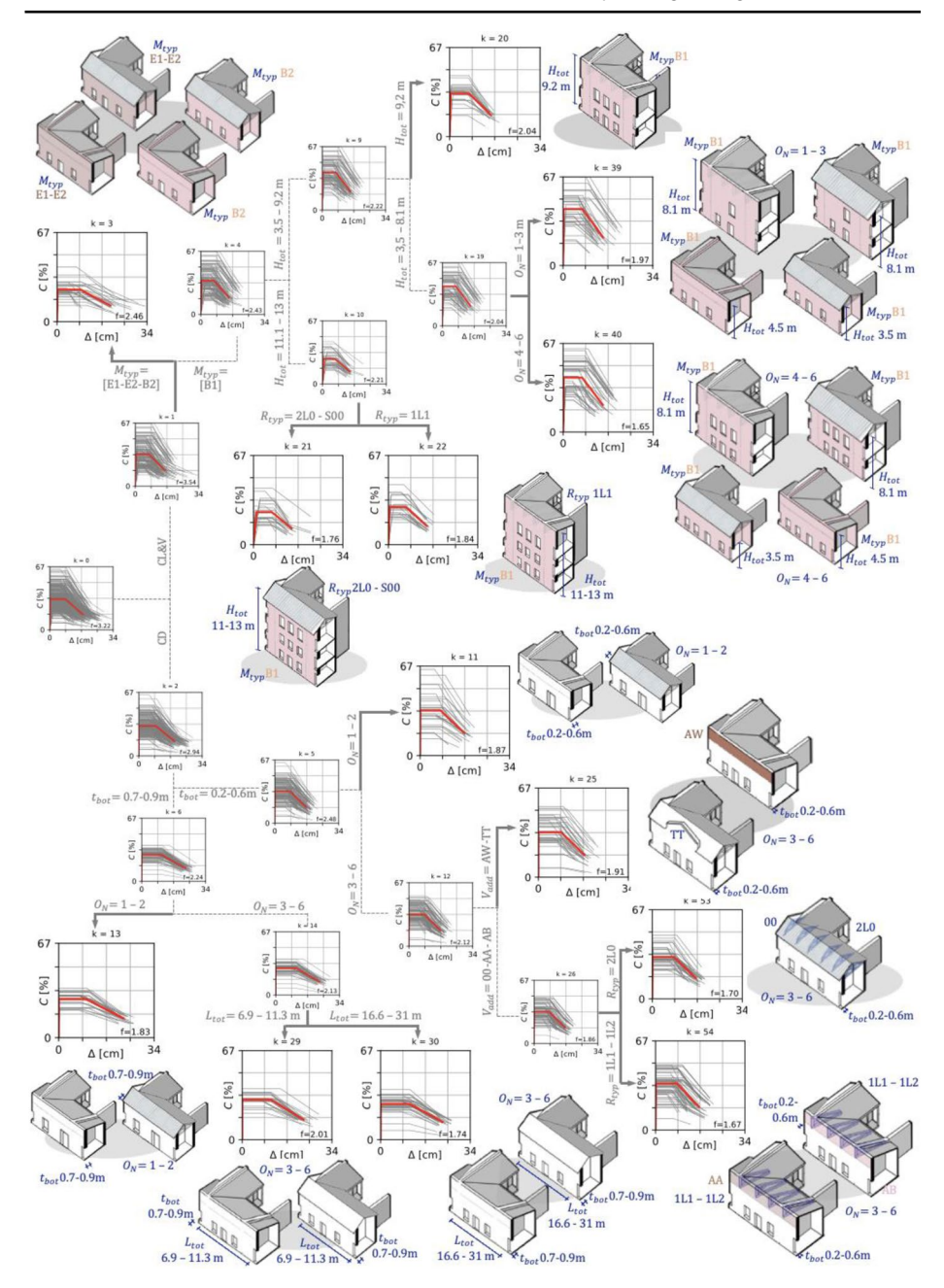


Fig. 12 Logic tree with the classification of the capacity curves



Clus-		Characterization	Mean capacity curve	Fit-
ter index	façades		A_u in [%g]	ness
muex			δ_{A_u} in [cm] δ_{A_c} in [cm]	[-]
3	29	Architectural style [-]=Classicist and variant Masonry type [-]= [E1, E2, B2]	$A_u = 24.2\delta_{A_u} = 8.8\delta_{A_c} = 20.2$	2.64
20	21	Architectural style [-]=Classicist and variant Masonry type [-]= [B1] Total height $[m]$ = $[x$ = 9.2]	$A_u = 32.5\delta_{A_u} = 7.3\delta_{A_c} = 15.5$	2.04
21	21	Architectural style [-]=Classicist and variant Masonry type [-]= $[B1]$ Total height $[m]$ = $[11.1 \le x \le 13.0]$ Roof type $[-]$ = $[1L1]$	$A_u = 24.5\delta_{A_u} = 7.0\delta_{A_c} = 14.5$	1.76
22	22	Architectural style [-]=Classicist and variant Masonry type [-]= $[B1]$ Total height $[m]$ = $[11.1 \le x \le 13.0]$ Roof type $[-]$ = $[2L0, S00]$	$A_u = 28.4\delta_{A_u} = 6.6\delta_{A_c} = 14.5$	1.84
39	36	Architectural style [-]=Classicist and variant Masonry type [-]= $[B1]$ Total height $[m]$ = $[3.5 \le x \le 8.1]$ Average number of openings per story $[-]$ = $[1 \le x \le 3]$	$A_u = 42.7\delta_{A_u} = 7.4\delta_{A_c} = 15.1$	1.97
40	41	Architectural style [-]=Classicist and variant Masonry type [-]= $[B1]$ Total height $[m]=[3.5 \le x \le 8.1]$ Average number of openings per story $[-]=[4 \le x \le 6]$	$A_u = 41.1\delta_{A_u} = 7.2\delta_{A_c} = 15.0$	1.65
11	28	Architectural style [-]=Colonial derivation Thickness at wall base [cm]= $[20 \le x \le 60]$ Average number of openings per story [-]= $[1 \le x \le 2]$	$A_u = 34.0\delta_{A_u} = 7.8\delta_{A_c} = 16.8$	1.87
13	26	Architectural style [-]=Colonial derivation Thickness at wall base [cm]= $[70 \le x \le 90]$ Average number of openings per story [-]= $[1 \le x \le 2]$	$A_u = 27.5\delta_{A_u} = 9.6\delta_{A_c} = 23.1$	1.83
25	38	Architectural style [-]=Colonial derivation Thickness at wall base [cm]= $[20 \le x \le 60]$ Average number of openings per story [-]= $[3 \le x \le 6]$ Vertical additions [-]= $[AW, TT]$	$A_u = 33.9\delta_{A_u} = 8.6\delta_{A_c} = 17.4$	1.91



Table 3	(continued))		
Clus-	Number of	Characterization	Mean capacity curve	Fit-
ter	façades		A_u in [%g]	ness
index			δ_{A_u} in [cm]	[-]
			δ_{A_c} in [cm]	
29	24	Architectural style [-]=Colonial derivation Thickness at wall base [cm]= $[70 \le x \le 90]$ Average number of openings per story [-]= $[3 \le x \le 6]$ Total length [m] = $[6.9 \le x \le 11.7]$	$A_u = 30.2\delta_{A_u} = 10.8\delta_{A_c} = 23.2$	2.01
30	37	Architectural style [-]=Colonial derivation Thickness at wall base [cm]= $[70 \le x \le 90]$ Average number of openings per story [-]= $[3 \le x \le 6]$ Total length [m]= $[16.6 \le x \le 31.0]$	$A_u = 26.9\delta_{A_u} = 11.0\delta_{A_c} = 23.4$	1.74
53	39	Architectural style [-]=Colonial derivation Thickness at wall base [cm]= $[20 \le x \le 60]$ Average number of openings per story [-]= $[3 \le x \le 6]$ Vertical additions [-]= $[00,\ AA,AB]$ Roof type [-]= $[2L0,2H0,S00]$	$A_u = 31.6\delta_{A_u} = 8.2\delta_{A_c} = 16.4$	1.70
54	61	Architectural style [-]=Colonial derivation Thickness at wall base [cm]= $[20 \le x \le 60]$ Average number of openings per story [-]= $[3 \le x \le 6]$ Vertical additions [-]= $[00, AA, AB]$ Roof type [-]= $[1L1, 1L2]$	$A_u = 34.9\delta_{A_u} = 8.2\delta_{A_c} = 16.5$	1.67

3.3 Derivation of fragility functions

Having obtained a set of typological capacity curves, the fragility assessment represents the next step in the FaMIVE methodology to determine the seismic response of these building typologies. Among various methods of deriving fragility functions, the N2 method (Fajfar and Dolšek 2012) incorporated in EC8 is adapted here by using idealized bilinear capacity curves, one for each of the curves in Fig. 13, against natural response spectra in the acceleration-displacement response spectral space (ADRS) to identify performance points expressed in terms of a coordinate intensity measure (IM) and an Engineering Design Parameter (EDP) (Dolšek and Fajfar 2004).

Considering the specific seismicity of Santiago del Chile, first, a seismic hazard curve was computed for the building site with the SeismicHazard platform (Candia et al. 2019), considering the coordinates for Santiago de Chile, a Vs30 comprised between 500 m/s and 900 m/s, in agreement with the soil classification type B (NCh433.Of1996 2009; Decreto



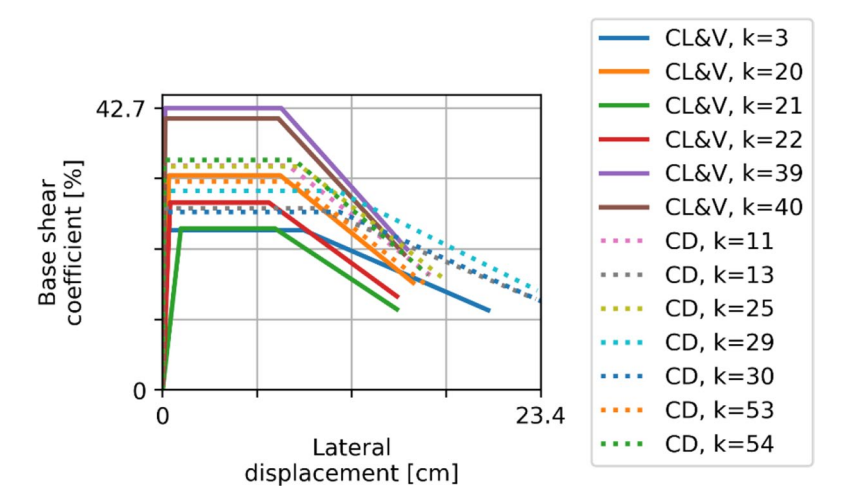


Fig. 13 Mean Capacity curves for the selected clusters

Supremo 2011). To derive the seismic hazard curve for the location, 5 ground motion prediction equations (GMPEs) were used (Zhao 2006; Montalva et al. 2017; Kuehn et al. 2020; Parker et al. 2022; Abrahamson and Gulerce 2022) equally weighted, together with the zonation and recurrence models developed by Poulos et al. (2019) and the scaling model by Strasser (2010). Secondly a target conditional spectrum was computed for each of 28 different hazard levels, corresponding to increasing return periods from 10 to 5000 years, using method 3 proposed by Lin et al. (2013) and the inter-period correlation model proposed by Candia et al (2020). Finally, following the method proposed by Baker and Lee (2018), 22 records were selected for each target Conditional Spectrum from the SIBER-RISK (Castro et al. 2022) strong-motion database, considering equal weights for median and standard deviation errors. For each ground motion, the horizontal components were considered as independent records since the analysis to be carried out requires only a single-component seismic record.

Considering that the capacity curves clustering procedure has proven to be susceptible to the ultimate and collapse displacements, the fragility functions are presented in terms of displacement and generated using the least square error method (D'Ayala et al. 2015) with a lognormal relationship between EDP and IM, by computing the median and standard deviation of the lognormal cumulative distribution through range-wise linear regression with respect to the performance levels defined: light (DS1), moderate (DS2), extensive (DS3) and collapse (DS4).

In determining the fragility functions it is essential to account for variability in both capacity and demand, in other words to account for the variance in the capacity curves included in each cluster, along with the variability in hazard, catered for by the suite of 22 spectra introduced above. It is noticeable that the variability in response capacity differs not just from cluster to cluster, which is considered by computing the mean capacity curve for each cluster, but, within a cluster, also from damage threshold to damage threshold. To account for this the dispersion calculated from the numerical analysis, $\beta_c(DS_i)$, is combined with the hazard dispersion $\beta_d(DS_i)$ computed for each damage state, by using Eq. 11:



$$\beta_{tot}\left(DS_{i}\right) = \sqrt[2]{\beta_{c}^{2}\left(DS_{i}\right) + \beta_{d}^{2}\left(DS_{i}\right)}$$
(11)

Therefore, fragility functions for the 4 performance levels for the 13 clusters are presented in Fig. 14 and in Table 4. The graphs show that the difference in performance between the typologies is preserved, especially for the advanced performance level of extensive damage and collapse. It may be noted that clusters 13, 29 and 30 have near zero probability of collapse for a displacement of 10 cm, which is explained by them having large wall thick-

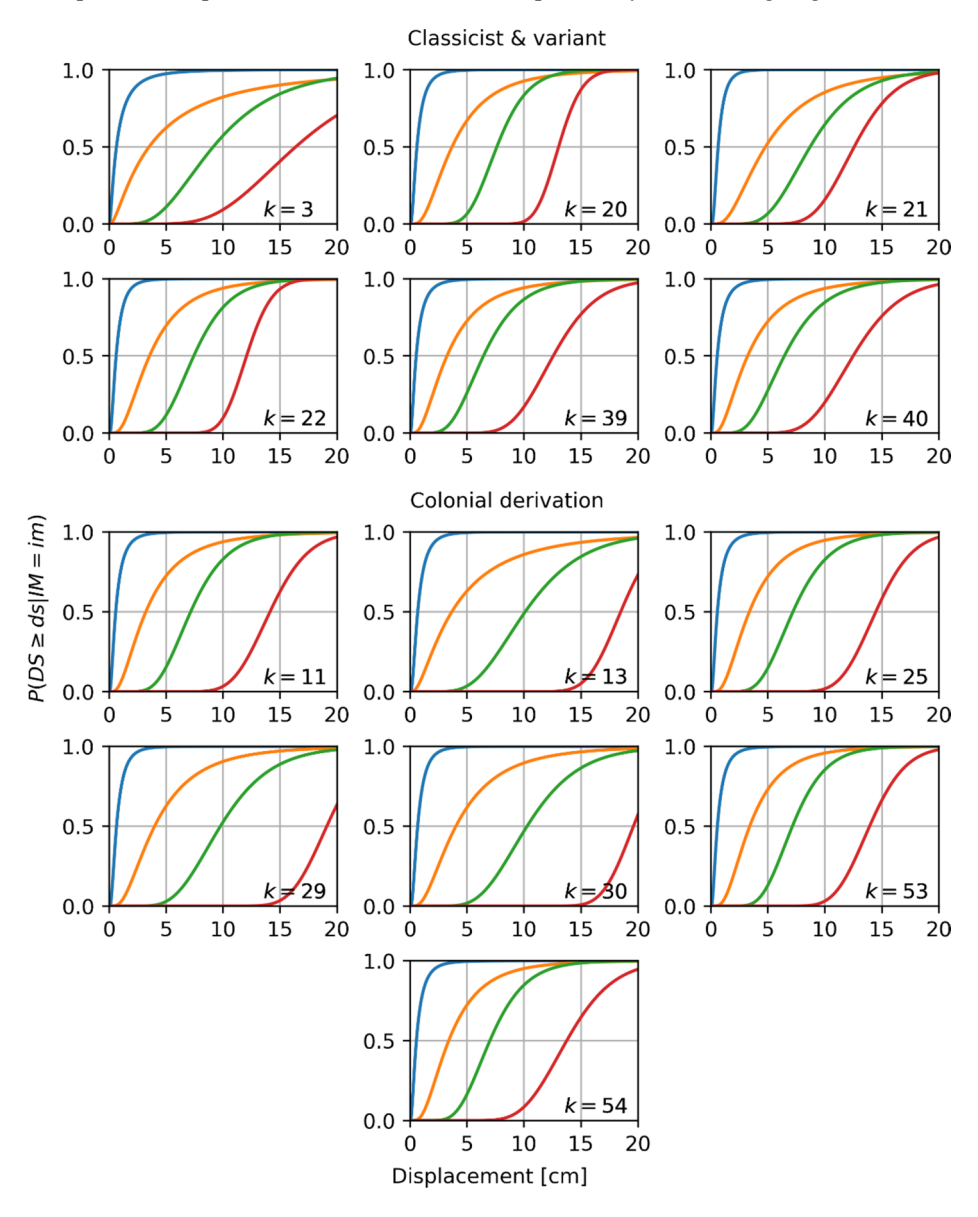


Fig. 14 Fragility functions for each cluster obtained by using a suite of natural response spectra



54

0.56

3.40

7.01

Style	Cluster	Mediar	$(\exp \theta)$	cm]		Log-star	Log-standard-deviation (β)				
		DS1	DS2	DS3	DS4	DS1	DS2	DS3	DS4		
CL	3	0.64	3.51	9.13	16.37	1.060	1.132	0.492	0.373		
	20	0.61	3.69	7.62	13.04	0.786	0.689	0.280	0.124		
	21	0.64	4.78	8.70	12.57	0.680	0.702	0.372	0.228		
	22	0.61	3.54	7.43	12.06	0.755	0.673	0.331	0.145		
	39	0.54	3.24	6.45	12.57	0.863	0.720	0.396	0.240		
	40	0.56	3.22	6.45	12.48	0.861	0.740	0.429	0.263		
	11	0.58	3.22	7.16	14.11	0.814	0.737	0.351	0.188		
CD	13	0.68	3.67	10.11	18.49	0.762	0.934	0.389	0.128		
	25	0.57	3.37	7.20	14.47	0.821	0.670	0.350	0.176		
	29	0.65	3.99	9.77	19.10	0.742	0.701	0.353	0.133		
	30	0.67	4.03	10.27	19.60	0.732	0.723	0.344	0.111		
	53	0.57	3.40	7.15	13.92	0.811	0.624	0.319	0.178		

Table 4 Summary of the median (exp θ) and log-standard-deviation (β) of the fragility functions

ness—in the range of 0.70 to 0.90 m—and being only one storey high, as can be seen in Fig. 12, hence their probability of overturning is very modest.

13.75

0.826

0.652

0.346

0.232

The obtained fragility functions are also shown in Fig. 15, where they are grouped by architectural style and Damage State, to ease comparison between clusters. It may be observed that fragility functions do not present important variations for DS1 for either architectural style, but they do differ for the other damage levels, although not for all clusters. In the case of Classicist and Variant style, cluster #3 (blue) differs from all others for all Damage States, and since it is obtained after the first branching and is not further divided, it highlights the importance of masonry type in seismic fragilities, since all other clusters correspond to masonry B1, while façades in cluster #3 have the other types. Cluster #21 (green) is also clearly different from the others, although not to the same extent throughout different Damage States. For instance, fragility functions are almost identical to clusters #39 (purple) and #40 (brown) for DS4, but this is not the case for DS2 and DS3. These three clusters share a common origin in cluster #9, differing in total height, which shows that while this parameter may not be important for the ultimate Damage State, it does change fragilities for intermediate ones. Finally, clusters #20 (yellow) and #22 (red) are almost identical for DS1 to DS3, and differ slightly for DS4. Since they correspond to subdivision of different clusters (#9 and #10, respectively), they cannot be combined to simplify the logic tree without combining all the other clusters except for #3, which would be inappropriate since fragility functions are sufficiently different, even with respect to cluster #21 (green), the complement of cluster #22. Therefore, the structure of the logic tree obtained for the capacity curves of Classicist and Variant façades is adequately preserved in the fragility functions outcome.

In the case of Colonial Derivation style, fragility functions are once again almost identical for DS1, while differences may be appreciated for higher Damage States. However, in this case the logic tree may be simplified by recombining in two main clusters if desired. Clusters #11 (blue), #25 (green), #53 (brown) and #54 (pink) may be aggregated into cluster #5, while clusters #13 (yellow), #29 (red) and #30 (purple) may be aggregated into cluster #6, their respective origin clusters. This indicates that the controlling parameter between these façades is the thickness of the wall at its base, and even though further subdivisions in the logic tree improve the classification of the capacity curves, this improvement is only



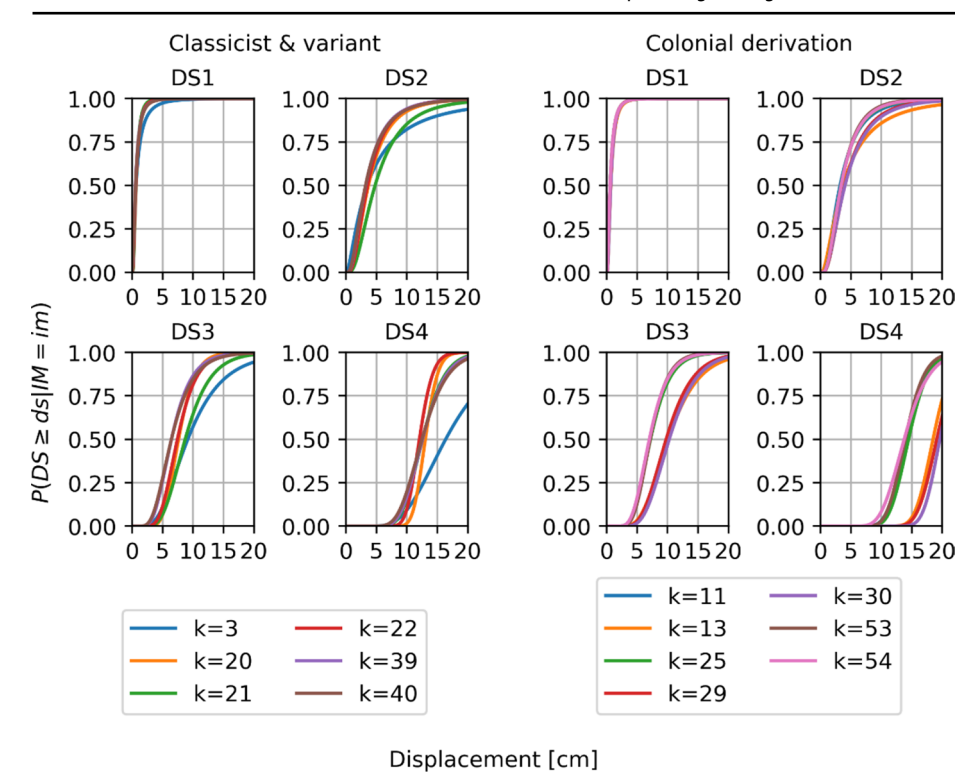


Fig. 15 Comparison of fragility functions by Architectural Style and Damage State

marginally reflected in the fragility functions. Therefore, the structure of the tree is preserved, however the subdivisions lead to capacity curves and fragility functions tat are not sufficiently differentiated.

4 Discussion and conclusions

Results presented in Section 3 show that the proposed methodology provide adequate typological fragility functions for aggregate unreinforced masonry façades of historical buildings in central Chile. Nonetheless, it is important to understand the capabilities and limitations of the algorithm. With this in mind, the method was applied multiple times with changes in some parameters. For instance, the weights considered for computing the fitness function for the classification algorithm were varied to change the relative importance of acceleration capacity (A_u) , ultimate deformation (δ_u) and collapse deformation (δ_c) . Although different combinations of weights produced similar Logic Trees of capacity curves, variations were more evident in the fragility functions of the clusters, where some combinations of weights produced distinguishable clusters only for some Damage States. For instance, it was observed that if the ultimate deformation was considered with a weight equal to zero, clusters could be easily identified for DS4, but not for other Damage States; while using a non-zero weight for δ_u produced clusters distinguishable for all Damage States but the first one. This is reasonable, since the highest damage state is greatly controlled by the deforma-



tion capacity, while in lower damage states the other parameters of the capacity curves are important. Ultimately, equal weights were considered because they produced good results for all Damage States. Nevertheless, weights were incorporated in the proposed algorithm to generalize the methodology.

Variations in other variables, such as maximum tree depth and fitness function tolerance mostly control overfitting. While the minimum number of elements per cluster also affected overfitting, interestingly it altered the order of the logic tree as well, since some of the decision variables were preserved, but swapped. In general terms, the obtained logic tree was very stable, and changes in the weights did not produce drastic variations in the results, since it was observed that decision variables tend to be the same, with some variations in the order of branching. To compare results with traditional statistics outputs, a correlation matrix was computed for the dataset containing both the façade properties and the capacity curve parameters. Figure 16 shows an extract of the correlation matrix for both architectural styles. It is observed that most of the correlations have intermediate values, but there are a few stronger ones, such as between wall thickness at the bottom (δ_u, δ_c) and ultimate/collapse displacement (β) , or number of stories/total height (N_{sto}) , (H_{tot}) and ultimate acceleration (A_u) . While it is not always the case, the logic tree tends to select façades properties highly correlated with capacity curve parameters as decision variables to divide the clusters, which partly explains the stability of the results.

The results obtained illustrate the flexibility of the proposed algorithm, since it allows the user to decide what aspects of seismic behavior are important for classification (e.g. only collapse displacement or other parameters of the capacity curve). Moreover, the formulation is sufficiently general to be applied to other problems, as it has successfully been applied to directly

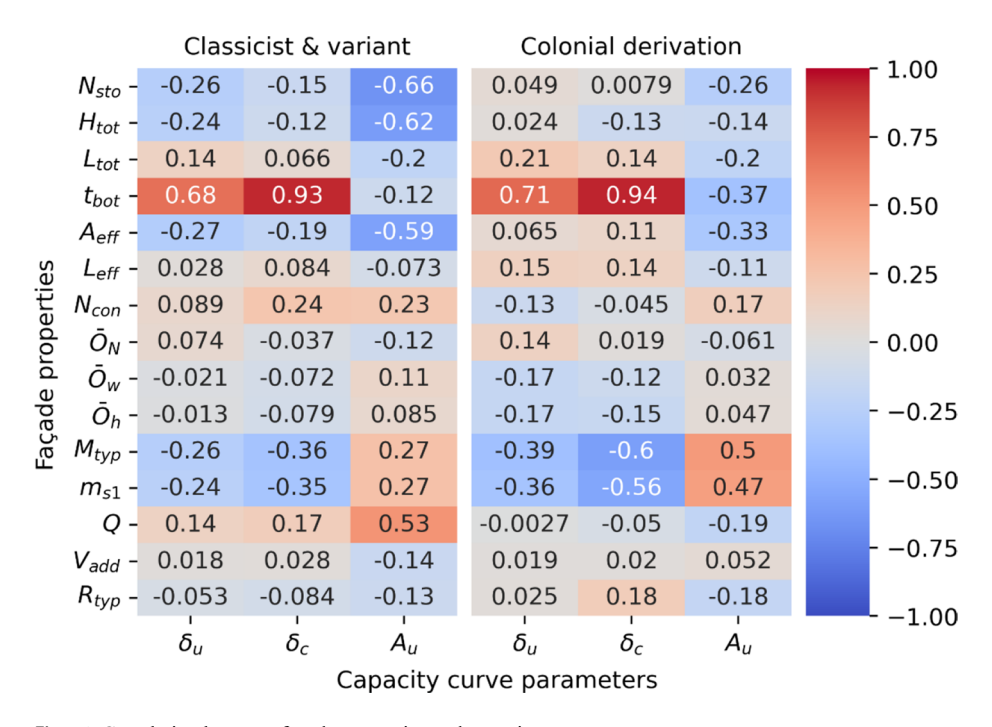


Fig. 16 Correlation between façade properties and capacity curve parameters



classify fragility functions of electric substations (Ahumada et al. 2025). The classification algorithm proved to be flexible and stable, nonetheless, future work may focus on improving its capabilities. For instance, more research is required to determine the optimal hyperparameters and to better understand how they impact on the obtained logic tree. The branching process may also be improved by considering additional information in the computation of the fitness function, such as the correlation matrix at each branching point. Finally, the methodology used to determine the optimal split at each node may be modified to increase the robustness of the algorithm, for example, by using backtracking to avoid getting trapped in local optima; or by considering global changes—in addition to already explained local ones—when constructing the Logic Tree to prevent obtaining unbalanced clusters in terms of uncertainty.

The seismic vulnerability analysis of the Yungay neighborhood using the FaMIVE method confirmed the intrinsic complexity of the data collection process in an urban, heritage, and historical context, particularly considering the inclusion of 43 urban blocks and 542 historic buildings. To address this complexity, a multi-strategy approach was adopted, combining fieldwork, archival analysis, and community engagement activities. A preliminary collection of geometric, construction, and structural data was carried out by consulting various archives, including the three Land Registers of the Illustrious Municipality of Santiago (1910, 1939, and 1960) and the Land Registers of the Chilean Income Tax System, through its Digital Cartography Maps (2025). This archival analysis was complemented and refined through an extensive field survey, requiring four months of work by a team of four specialized professionals (two architects and two engineers). Additionally, two community meetings were held with the Yungay Neighborhood Council to present and discuss the project, fostering the support and active participation of residents. These community engagement activities were essential, as they not only informed the community but also encouraged their active involvement, enriching the process and ensuring its successful execution, by granting access to properties and aiding the data collection process.

The heterogeneity of construction features, the evolution of urban regulations, and the retrofitting interventions implemented over time added further layers of complexity. These challenges were addressed through sensitivity analyses to account for uncertainties in parameters such as wall thickness, structural connections, and material properties. This comprehensive approach not only enabled the identification of predominant collapse mechanisms but also provided critical insights for prioritizing seismic mitigation interventions tailored to the historical and cultural context of the neighborhood.

Results obtained from this study can be effectively extrapolated to evaluate the seismic behavior of heritage buildings in other historic urban areas in Chile and, potentially, in other historic neighborhoods across Latin America, particularly those that share a common historic and urban origin. This generalizability is underpinned by the fact that the urban and architectural layouts of many Chilean and Latin American cities were governed by the planning principles codified in the first city planning ordinances—the Laws of the Indies issued by the Spanish Crown (Ministerio de la Vivienda 1973). These ordinances prescribed a characteristic urban morphology, including 'a central square plaza with eight streets radiating from its corners, buildings of uniform typology, continuous façades, large yards, and corrals' (Ministerio de la Vivienda 1973). Given the analogous construction typologies, architectural features, and urban planning traditions, the methodologies and findings of this study provide a rigorous and adaptable framework for assessing seismic vulnerability in similar contexts. Nevertheless, to ensure accurate application, regional specificities in construction materials, seismic hazard profiles, and retrofitting practices must be carefully accounted for.



With this consideration, it is possible to extend to other contexts both main outcomes of this study, namely, (1) a set of analytical fragility functions (AFFs) that characterize the seismic performance of clusters of URM buildings in the Yungay quarter; and (2) a methodological framework that integrates the FaMIVE approach with an optimized logic tree analysis (LTA) for classification based on observable architectural features.

Regarding the fragility functions, these can be meaningfully extended to other historic neighborhoods in Chile and Latin America that share similar morphological and constructive features with Yungay. Examples include Franklin or La Chimba in Santiago (Chile), the Barrio San Juan Moyotlan in Mexico City (Mexico), or La Guaragua in Quito (Ecuador). These urban fabrics exhibit comparable typologies of unreinforced masonry buildings, developed through similar historical processes and characterized by high structural heterogeneity, informal transformations, and the absence of seismic-specific detailing. In this sense, the AFFs derived in our study offer a valuable benchmark for prioritizing risk mitigation strategies in such analogous contexts.

On the other hand, the FaMIVE+LTA methodology is designed to be more broadly applicable, even in historic urban contexts beyond Latin America. FaMIVE has already been applied to numerous historic urban context in Europe, Africa and Asia, thanks to its flexibility in adapting the input data to the local construction practice and in easily coding the solvers to take into account specific collapse mechanisms associated with local construction deficiencies. On the other hand, the logic tree algorithm does not rely on region-specific classifications, but on clustering based on observable features, which are not hardcoded and can therefore be adapted to different architectural and construction traditions, the same used to compute the collapse mechanisms and the capacity curves. Of course, minor adaptations may be required when computing capacity curves and fragility functions, to reflect the specific material, structural, and morphological characteristics of the new context. Nonetheless, the methodological logic remains transferable.

5 Annex A: Mechanical properties of masonry

5.1 Masonry types B1 and B2

Two representative samples were extracted from façades of the Yungay quarter and subjected to different tests to estimate mechanical properties of masonry, including compression tests on bricks and mortar (both samples), split cylinder tests on masonry cores (only sample B1), and cohesion coefficient measurements between bricks and mortar (both samples), as shown in Fig. 17. One specimen was extracted from a structure built in Masonry Type B1 (1-leaf brickwork), while a second specimen corresponded to Masonry Type B2 (2-leaf brickwork), as depicted in Fig. 18. The results obtained are presented in the next three subsections for both masonry types considered.





Fig. 17 Compression strength test (left), tensile strength test (center), and cohesion coefficient test (right)

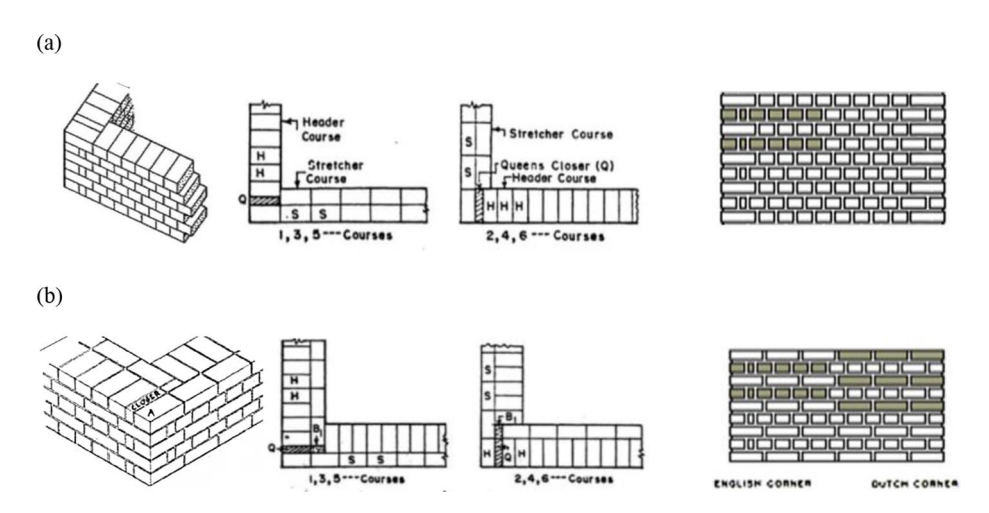


Fig. 18 Masonry types where samples were extracted. (a) Masonry type B1: 1-leaf brickwork; and (b) Masonry type B2: 2-leaf brickwork

5.1.1 Compression strength test of brick and mortar

Obtained results are presented in Table 5 and Fig. 19 for samples B1 and B2.

Table 5 Results of compression strength test for sample B1 and B2

Sample N°	Width1 [mm]	Width2 [mm]	High [mm]	Mortal thick. [mm]	Area [mm2]	Max. Load [kN]	Max. load deform. [mm]	Compres. strength [MPa]
B1	196	194	81	26	38,024	159.7	2.92	4.2
B2	189	200	85	24	37,800	288.3	5.71	7.6





Fig. 19 Results of compression strength test of samples B1 (blue) and B2 (orange)

5.1.2 Tensile strength test of masonry

Obtained results are presented in Table 6 and Fig. 20 for sample B1.

Table 6 Results of split cylinder test for sample B1

Sample N°	Width1 [mm]	Diam. [mm]	High [mm]	Mortal thick. [mm]	Area [mm2]	Max. Load [kN]	Max. load deform. [mm]	Tensile strength [MPa]
1	215	150	-	30	-	18.2	4.7	0.36



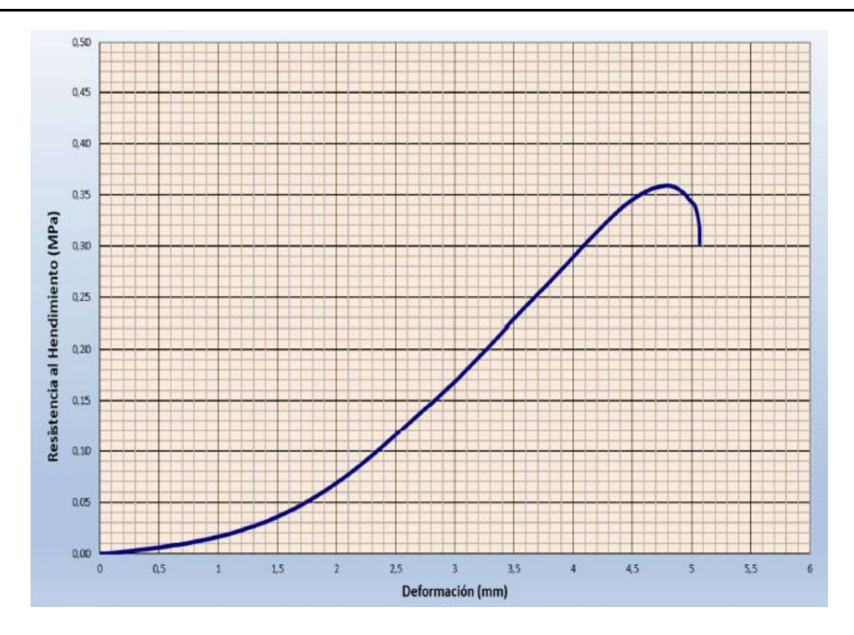


Fig. 20 Results of tensile strength test for sample B1

5.1.3 Cohesion coefficient brick-mortar

Results are presented in Table 7 and Fig. 21 for samples B1 and B2.

Table 7 Results of cohesion coefficient for samples B1 and B2

iubic / ite	barts of con	esion coem	ciciii ioi bu	inpies Di un	u D2			
Sample N°	Width1 [mm]	Diam. [mm]	High [mm]	Mortal thick. [mm]	Area [mm2]	Max. Load [kN]	Max. load deform. [mm]	Cohesion coeff. [MPa]
1	132	150	-	33	37,084	11.37	0.82	0.31
2	120	150	-	26	34,320	9.58	0.84	0.28



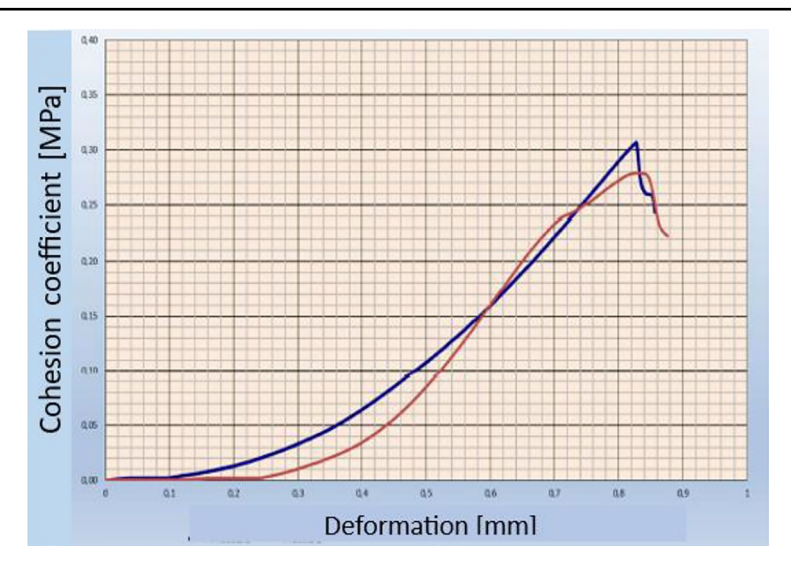


Fig. 21 Results of cohesion coefficient for samples B1 (blue) and B2 (orange)

5.2 Adobe masonry type E1 and E2

Direct material testing was not feasible within the scope of this study for adobe masonry wall (Fig. 22), therefore, mechanical properties were obtained from Chilean (NCh3332:2013 2013) and Peruvian [61] standards, as well as from a related thesis (Gonzales and Edwards 2016). Considered values are presented in Table 8.







Fig. 22 Typical adobe masonry in the Yungay quarter

 Table 8 Considered mechanical

 parameters for adobe masonry

Material property	Unit	Value	Source
Compressive strength	MPa	1.2	NCh3332:2013
Modulus of elasticity	MPa	200	NCh3332:2013
Tensile strength	MPa	0.025	NCh3332:2013
Density	Kg/m3	1660	In situ testing
Friction	Degrees	28.5°-35°	E80, Gonzales and Edwards 2016
Cohesion coefficient	MPa	0.038-0.045	Gonzales and Edwards 2016

Acknowledgements The authors gratefully acknowledge the collaboration of architects Elena Ávila Serrano and Marco Barrientos, as well as engineers Bruno Ruiz and Graciela Ramírez, for their valuable contributions to the field surveys. The authors also extend their sincere thanks to José Osorio (Executive Director of the Asociación Chilena de Barrios y Zonas Patrimoniales) and the Second Fire Company of Santiago 'Esmeralda' for their support in data collection and their collaboration in organizing community consultations. The strong motion database was provided by the SIBER-RISK project: Simulation Based Earthquake Risk and Resilience of Interdependent Systems and Networks ANID/FONDECYT/1170836. https://doi.org/10.7764/datasetUC/ING-UC.1170836 1.

Author contributions Juan Pablo Muñoz: methodology, software, formal analysis, data curation, writing – original draft, writing – review & editing, visualization, funding acquisition, project administration. Dina



D'Ayala: Conceptualization, methodology, software, validation, formal analysis, resources, data curation, writing – original draft, writing – review & editing, visualization, supervision, funding acquisition. Nuria Chiara Palazzi: Conceptualization, methodology, software, formal analysis, investigation, resources, data curation, writing – original draft, writing – review & editing, visualization, funding acquisition. Juan Carlos de la Llera: Conceptualization, methodology, writing – review & editing, supervision, funding acquisition.

Funding This work was supported by the Research Center for Integrated Disaster Risk Management (CIGIDEN) ANID/FONDAP/1523A0009, the research project "Multiscale earthquake risk mitigation of healthcare networks using seismic isolation" ANID/FONDECYT/1220292, the research grant Nucleos/UNAB/2024/81360982 of Universidad Andrés Bello, and the joint research project "Seismic risk analysis of Historic Urban Areas: An application to the Yungay Neighborhood in Santiago, Chile" granted by the Strategic Partner Funds between Pontificia Universidad Católica de Chile and University College London. The authors are grateful for this support.

Data availability The datasets generated and/or analysed during the current study are available from the corresponding author on reasonable request.

Declarations

Competing interests The authors have no relevant financial or non-financial interests to disclose.

Open Access This article is licensed under a Creative Commons Attribution 4.0 International License, which permits use, sharing, adaptation, distribution and reproduction in any medium or format, as long as you give appropriate credit to the original author(s) and the source, provide a link to the Creative Commons licence, and indicate if changes were made. The images or other third party material in this article are included in the article's Creative Commons licence, unless indicated otherwise in a credit line to the material. If material is not included in the article's Creative Commons licence and your intended use is not permitted by statutory regulation or exceeds the permitted use, you will need to obtain permission directly from the copyright holder. To view a copy of this licence, visit http://creativecommons.org/licenses/by/4.0/.

References

- Abrahamson NA, Gulerce Z (2022) Summary of the Abrahamson and Gulerce NGA-SUB ground-motion model for subduction earthquakes. Earthq Spectra 38:2638–2681. https://doi.org/10.1177/87552930221114374
- Adhikari RK, D'Ayala D (2020) Nepal earthquake: Seismic performance and post-earthquake reconstruction of stone in mud mortar masonry buildings. Bull Earthq Eng 18:3863–3896. https://doi.org/10.1007/s10518-020-00834-y
- Ahumada N, Poulos A, De La Llera JC, Muñoz JP, Rojas F (2025) Seismic fragility estimation of electrical substations accounting for component damage and short circuit faults (under revision). Reliab Eng Syst Saf
- Angiolilli M, Lagomarsino S, Cattari S, Degli Abbati S (2021) Seismic fragility assessment of existing masonry buildings in aggregate. Eng Struct 247:113218. https://doi.org/10.1016/j.engstruct.2021.113 218
- Baker JW, Lee C (2018) An improved algorithm for selecting ground motions to match a conditional spectrum. J Earthq Eng 22:708–723. https://doi.org/10.1080/13632469.2016.1264334
- Basaglia A, Aprile A, Spacone E, Pilla F (2018) Performance-based seismic risk assessment of urban systems. Int J Archit Herit 12:1131–1149. https://doi.org/10.1080/15583058.2018.1503371
- Benedetti, D., Petrini, V. (1984) On the seismic vulnerability of masonry buildings: an evaluation method (in Italian). 149:66–74
- Bertolesi E, Milani G, Casolo S (2018) Homogenization towards a mechanistic rigid body and spring model (HRBSM) for the non-linear dynamic analysis of 3D masonry structures. Meccanica 53:1819–1855. https://doi.org/10.1007/s11012-017-0665-6
- Betti M, Galano L, Vignoli A (2014) Comparative analysis on the seismic behaviour of unreinforced masonry buildings with flexible diaphragms. Eng Struct 61:195–208. https://doi.org/10.1016/j.engstruct.2013.1 2.038



- Bhattacharjee P, Mitra P (2021) A survey of density based clustering algorithms. Front Comput Sci 15:151308. https://link.springer.com/10.1007/s11704-019-9059-3
- Bosiljkov V, D'Ayala D, Novelli V (2015) Evaluation of uncertainties in determining the seismic vulnerability of historic masonry buildings in Slovenia: use of macro-element and structural element modelling. Bull Earthq Eng 13:311–329. https://doi.org/10.1007/s10518-014-9652-7
- Braga F, Dolce M, Liberatore D (1982) A statistical study on damaged buildings and ensuing review of the MSK-76 SCALE. In Proceedings of the 7th European Conference on Earthquake Engineering. Athens, Greece
- Brando G, De Matteis G, Spacone E (2017) Predictive model for the seismic vulnerability assessment of small historic centres: Application to the inner Abruzzi region in Italy. Eng Struct 153:81–96. https://doi.org/10.1016/j.engstruct.2017.10.013
- Candia G, Macedo J, Jaimes MA, Magna-Verdugo C (2019) A new state-of-the-art platform for probabilistic and deterministic seismic hazard assessment. Seismol Res Lett 90:2262–2275. https://doi.org/10.1785 /0220190025
- Candia G, Poulos A, de la Llera JC, Crempien JGF, Macedo J (2020) Correlations of spectral accelerations in the Chilean subduction zone. Earthq Spectra 36:788–805. https://doi.org/10.1177/8755293019891723
- Cardinali V et al (2022) A multiscale approach for the seismic vulnerability assessment of historical centres in masonry building aggregates: Cognitive approach and interdisciplinary perspectives. Int J Archit Herit 16:839–864. https://doi.org/10.1080/15583058.2021.1992536
- Carocci CF (2012) Small centres damaged by 2009 L'Aquila earthquake: on site analyses of historical masonry aggregates. Bull Earthq Eng 10:45–71. https://doi.org/10.1007/s10518-011-9284-0
- Castro S, Benavente R, Crempien JGF, Candia G, de la Llera JC (2022) A consistently processed strong-motion database for Chilean earthquakes. Seismol Res Lett.. https://doi.org/10.1785/0220200336
- Colombi M et al (2008) Deriving vulnerability curves using Italian earthquake damage data. Bull Earthq Eng 6:485–504. https://doi.org/10.1007/s10518-008-9073-6
- Consejo de Monumentos Nacionales (2000) Decree 217 Declara zona típica los pasajes Lucrecia Valdés de Barros, Adriana Cousiño, Hurtado Rodríguez y calle aledañas, ubicados en la comuna de Santiago, provincia de Santiago, Región Metropolitana
- Consejo de Monumentos Nacionales (2009) Decree 43 Declárese monumento nacional en la categoría de zona típica o pintoresca el sector que indica de los barrios Yungay y Brasil de Santiago Poniente, de la cuidad de Santiago, Comuna y Provincia de, Santiago, Región Metropolitana
- Consejo de Monumentos Nacionales (2019) Decree 13 Modifica decreto nº 43, de 2009, del ministerio de educación que monumento nacional en la categoría de zona típica o pintoresca el sector que indica de los barrios Yungay y Brasil de Santiago Poniente, de la Cuidad de Santiago. Comuna Y Provincia de Santiago
- Da Porto F, Munari M, Prota A, Modena C (2013) Analysis and repair of clustered buildings: Case study of a block in the historic city centre of L'Aquila (Central Italy). Constr Build Mater 38:1221–1237. https://doi.org/10.1016/j.conbuildmat.2012.09.108
- D'Ayala D (2013) Assessing the seismic vulnerability of masonry buildings. In: Handbook of seismic risk analysis and management of civil infrastructure systems. Elsevier, pp 334–365.. https://doi.org/10.153 3/9780857098986.3.334
- D'Ayala D et al (2015) Guidelines for analytical vulnerability assessment low-mid rise. https://cloud-stora ge.globalquakemodel.org/public/wix-new-website/pdf-collections-wix/publications/Guidelines%20for %20Analytical%20Vulnerability%20Assessment%20-%20Low Mid-Rise.pdf
- D'Ayala D, Benzoni G (2012) Historic and traditional structures during the 2010 chile earthquake: Observations, codes, and conservation strategies. Earthq Spectra 28:425–451. https://doi.org/10.1193/1.4000030
- D'Ayala D, Kansal A (2004) Analysis of the seismic Vulnerability of the architectural heritage in Buhj. Gujarat, India. Proceedings of the Structural Analysis of Historical Construction Conference at Padova, Italy
- D'Ayala D, Speranza E (2003) Definition of collapse mechanisms and seismic vulnerability of historic masonry buildings. Earthq Spectra 19:479–509. https://doi.org/10.1193/1.1599896
- D'Ayala D, Yeomans D (2004) Assessing the seismic vulnerability of late ottoman buildings in Istanbul. Proceedings of the Structural analysis of historical construction Conference at Padova, Italy
- D'ayala D (2005) Force and displacement based vulnerability assessment for traditional buildings. Bull Earthq Eng 3:235-265. https://doi.org/10.1007/s10518-005-1239-x
- D'Ayala D, Paganoni S (2011) Assessment and analysis of damage in L'Aquila historic city centre after 6th april 2009. Bull Earthq Eng 9:81–104. https://doi.org/10.1007/s10518-010-9224-4
- Dolšek M, Fajfar P (2004) Inelastic spectra for infilled reinforced concrete frames. Earthq Engng Struct Dyn 33:1395–1416. https://doi.org/10.1002/eqe.410
- Fajfar P, Dolšek M (2012) A practice-oriented estimation of the failure probability of building structures. Earthq Engng Struct Dyn 41:531–547. https://doi.org/10.1002/eqe.1143



- Fajfar P, Gašperšič P (1996) The N2 method for the seismic damage analysis of RC buildings. Earthq Engng Struct Dyn 25:31–46. https://onlinelibrary.wiley.com/doi/abs/10.1002/%28SICI%291096-9845%2819 9601%2925%3A1%3C31%3A%3AAID-EOE534%3E3.0.CO%3B2-V
- Ferreira TM, Vicente R, Mendes Da Silva JAR, Varum H, Costa A (2013) Seismic vulnerability assessment of historical urban centres: case study of the old city centre in Seixal, Portugal. Bull Earthq Eng 11:1753–1773. https://doi.org/10.1007/s10518-013-9447-2
- Formisano A, Ademovic N (2022) An overview on seismic analysis of masonry building aggregates. Front Built Environ 8:966281. https://doi.org/10.3389/fbuil.2022.966281
- Gonzales B, Edwards J (2016) Determinación experimental de las propiedades de cohesión y ángulo de fricción de la mampostería de adobe, piedra y ladrillo en edificaciones históricas peruanas. Pontificia Universidad Católica del Perú. http://hdl.handle.net/20.500.12404/7289
- Greco A, Lombardo G, Pantò B, Famà A (2020) Seismic vulnerability of historical masonry aggregate buildings in oriental sicily. Int J Archit Herit 14:517–540. https://doi.org/10.1080/15583058.2018.1553075
- Grillanda N, Valente M, Milani G, Chiozzi A, Tralli A (2020) Advanced numerical strategies for seismic assessment of historical masonry aggregates. Eng Struct 212:110441. https://doi.org/10.1016/j.engstr uct.2020.110441
- Guardiola Villora A, D'Ayala D, Pérez-García A (2024) FaMIVE shell 2024. https://www.ucl.ac.uk/epicent re/unesco-chair/famive
- Guardiola-Víllora A, Molina S, D'Ayala D (2023) Performance based probabilistic seismic risk assessment for urban heritage. An example in pla del remei area (Valencia). Bull Earthq Eng 21:4951–4991. https://doi.org/10.1007/s10518-023-01721-y
- Ikotun AM, Ezugwu AE, Abualigah L, Abuhaija B, Heming J (2023) K-means clustering algorithms: A comprehensive review, variants analysis, and advances in the era of big data. Inf Sci 622:178–210. https://doi.org/10.1016/j.ins.2022.11.139
- Instituto Nacional de Normalización (2013) NCh3332:2013 Estructuras intervención de construcciones patrimoniales de tierra cruda requisitos del proyecto estructural
- Instituto Nacional de Normalización (2009) NCh433.Of1996 Diseño sísmico de edificios
- Jaiswal K, Wald D, D'Ayala D (2011) Developing empirical collapse fragility functions for global building types. Earthq Spectra 27:775–795. https://doi.org/10.1193/1.3606398
- Kalkbrenner P, Pelà L, Sandoval C (2019) Multi directional pushover analysis of irregular masonry buildings without box behavior. Eng Struct 201:109534. https://doi.org/10.1016/j.engstruct.2019.109534
- Kircher CA, Nassar AA, Kustu O, Holmes WT (1997) Development of building damage functions for earth-quake loss estimation. Earthq Spectra 13:663–682. https://doi.org/10.1193/1.1585974
- Kuehn N, Bozorgonia Y, Campbell K, Gregor N (2020) Partially non-ergodic ground-motion model for subduction regions using the NGA-subduction database.. https://peer.berkeley.edu/publications/2020-04
- Lagomarsino S, Giovinazzi S (2006) Macroseismic and mechanical models for the vulnerability and damage assessment of current buildings. Bull Earthq Eng 4:415–443. https://doi.org/10.1007/s10518-006-9024-z
- Lagomarsino S, Penna A, Galasco A, Cattari S (2013) TREMURI program: An equivalent frame model for the nonlinear seismic analysis of masonry buildings. Eng Struct 56:1787–1799. https://doi.org/10.101 6/j.engstruct.2013.08.002
- Leggieri V, Ruggieri S, Zagari G, Uva G (2021) Appraising seismic vulnerability of masonry aggregates through an automated mechanical-typological approach. Autom Constr 132:103972. https://doi.org/10.1016/j.autcon.2021.103972
- Lin T, Harmsen SC, Baker JW, Luco N (2013) Conditional spectrum computation incorporating multiple causal earthquakes and ground-motion prediction models. Bull Seismol Soc Am 103:1103–1116. https://doi.org/10.1785/0120110293
- Lourenço PB, Mendes N, Ramos LF, Oliveira DV (2011) Analysis of masonry structures without box behavior. Int J Archit Herit 5:369–382. https://doi.org/10.1080/15583058.2010.528824
- Maimon O, Rokach L (2005) Data mining and knowledge discovery handbook. Springer, New York
- Maio R, Ferreira TM, Vicente R (2018) A critical discussion on the earthquake risk mitigation of urban cultural heritage assets. Int J Disaster Risk Reduct 27:239–247. https://doi.org/10.1016/j.ijdrr.2017.10.010
- Maio R, Ferreira TM, Vicente R, Estêvão J (2016) Seismic vulnerability assessment of historical urban centres: case study of the old city centre of Faro, Portugal. J Risk Res 19:551–580. https://doi.org/10.108 0/13669877.2014.988285
- Maio R, Vicente R, Formisano A, Varum H (2015) Seismic vulnerability of building aggregates through hybrid and indirect assessment techniques. Bull Earthq Eng 13:2995–3014. https://doi.org/10.1007/s1 0518-015-9747-9
- Martinelli A et al (2008) Building vulnerability assessment and damage scenarios in Celano (Italy) using a quick survey data-based methodology. Soil Dyn Earthq Eng 28:875–889. https://doi.org/10.1016/j.soildyn.2008.03.002



- Ministerio de la Vivienda (1973) El orden que se ha de tener en descubrir y poblar, transcripción de las ordenanzas de descubrimiento, nuevo población y pacificación de las Indias dadas por Felipe II, el 13 de julio de 1573, en el Bosque de Segovia, Archivo General de Indias de Sevilla
- Ministerio de Vivienda y Urbanismo (2011) Decreto Supremo 61
- Ministerio de Vivienda, Construcción y Saneamiento (2017) Norma E80 Diseño y construcción con tierra reforzada
- Montalva GA, Bastías N, Rodriguez-Marek A (2017) Ground-motion prediction equation for the chilean subduction zone. Bull Seismol Soc Am 107:901–911. https://doi.org/10.1785/0120160221
- Novelli VI, D'Ayala D, Makhloufi N, Benouar D, Zekagh A (2015). A procedure for the identification of the seismic vulnerability at territorial scale. Application to the Casbah of Algiers. Bull Earthq Eng 13:pp.177–202. https://doi.org/10.1007/s10518-014-9666-1
- Orsini G (1999) A model for buildings' vulnerability assessment using the parameterless scale of seismic intensity (PSI). Earthq Spectra 15:463–483. https://doi.org/10.1193/1.1586053
- Palazzi NC et al (2023) Fire risk assessment of historic urban aggregates: an application to the Yungay neighborhood in Santiago, Chile. Int J Disaster Risk Reduct 86:103550. https://doi.org/10.1016/j.ijdrr .2023.103550
- Palazzi NC, Amoruso G, Baquedano-Juliá P, Ferreira TM (2024) On the role of planning policies in the seismic vulnerability of historic urban areas: evidence from Santiago, Chile. Bull Earthq Eng 22:5891– 5916. https://doi.org/10.1007/s10518-024-01995-w
- Palazzi NC, Barrientos M, Sandoval C, de la Llera JC (2022) Seismic vulnerability assessment of the Yungay's historic urban center in Santiago, Chile. J Earthq Eng 1–28.. https://doi.org/10.1080/13632469. 2022.2087793
- Paquette J, Bruneau M (2006) Pseudo-dynamic testing of unreinforced masonry building with flexible diaphragm and comparison with existing procedures. Constr Build Mater 20:220–228. https://doi.org/10.1016/j.conbuildmat.2005.08.025
- Parker GA, Stewart JP, Boore DM, Atkinson GM, Hassani B (2022) NGA-subduction global ground motion models with regional adjustment factors. Earthq Spectra 38:456–493. https://doi.org/10.1177/8755293 0211034889
- Poulos A, Monsalve M, Zamora N, de la Llera JC (2019) An updated recurrence model for chilean subduction seismicity and statistical validation of its poisson nature. Bull Seismol Soc Am 109:66–74. https://doi. org/10.1785/0120170160
- Putrino V, D'Ayala D (2019a) Effectiveness of seismic strengthening to repeated earthquakes in historic urban contexts: Norcia 2016. DPM 29:47–64. https://doi.org/10.1108/DPM-07-2018-0230
- Putrino V, D'Ayala D (2019b) Norcia and amatrice: A comparison of the two historic centres' performance under the central Italy earthquake sequence. In Proceedings of the 7th International Conference on Computational Methods in Structural Dynamics and Earthquake Engineering (COMPDYN 2015). Institute of Structural Analysis and Antiseismic Research School of Civil Engineering National Technical University of Athens (NTUA), Greece, Crete, Greece, 2636–2648. doi:https://doi.org/10.7712/120 119.7099.19080
- Python Software Foundation (2025). https://docs.python.org/3/reference/index.html
- Ran X, Xi Y, Lu Y, Wang X, Lu Z (2023) Comprehensive survey on hierarchical clustering algorithms and the recent developments. Artif Intell Rev 56:8219–8264. https://doi.org/10.1007/s10462-022-10366-3
- Rapone D, Brando G, Spacone E, De Matteis G (2018) Seismic vulnerability assessment of historic centers: description of a predictive method and application to the case study of scanno (Abruzzi, Italy). Int J Archit Herit 12:1171–1195. https://doi.org/10.1080/15583058.2018.1503373
- Restrepo-Vélez LF, Ma genes G (2004) Simplified procedure for the seismic risk assessment of unreinforced masonry buildings. In Proceedings of the 13th World Conference on Earthquake Engineering. Vancouver, Canada, 2561
- Rossetto T, Ioannou I, Grant D (2014) Guidelines for empirical vulnerability assessment.. https://doi.org/10.13117/GEM.VULN-MOD.TR2014.11
- Rota M, Penna A, Strobbia C (2006) Typological fragility curves from Italian earthquake damage data. In: Proceedings of the 1st European conference on earthquake engineering and seismology. Geneva, 386
- Ruggieri S et al (2023) An archetype-based automated procedure to derive global-local seismic fragility of masonry building aggregates: META-FORMA-XL. Int J Disaster Risk Reduct 95:103903. https://doi.org/10.1016/j.ijdrr.2023.103903
- Schiavoni M, Giordano E, Roscini F, Clementi F (2023) Advanced numerical insights for an effective seismic assessment of historical masonry aggregates. Eng Struct 285:115997. https://doi.org/10.1016/j.engstru ct.2023.115997
- Servicio de Impuestos Internos (2025) Cartografía digital SII Mapas. Cartografía Digital SII Mapas.. https://www4.sii.cl/mapasui/internet/



- Singhal A, Kiremidjian A (2004) Empirical fragility functions from recent earthquakes. In: Proceedings of the 13th World Conference on Earthquake Engineering. Vancouver, Canada, 1211
- Singhal A, Kiremidjian AS (1998) Bayesian updating of fragilities with application to RC frames. J Struct Eng 124:922–929. https://ascelibrary.org/doi/10.1061/%28ASCE%290733-9445%281998%29124%3 A8%28922%29
- Strasser FO, Arango MC, Bommer JJ (2010) Scaling of the source dimensions of interface and intraslab subduction-zone earthquakes with moment magnitude. Seismol Res Lett 81:941–950. https://doi.org/10.1785/gssrl.81.6.941
- Tomić I, Vanin F, Beyer K (2021) Uncertainties in the seismic assessment of historical masonry buildings. Appl Sci 11:2280. https://doi.org/10.3390/app11052280
- Tosto C, Leggieri V, Ruggieri S, Uva G (2025) A multisource methodology for the regional seismic fragility assessment of existing masonry buildings in historical centres. Int J Archit Herit 1–26.. https://doi.org/10.1080/15583058.2025.2461119
- Valente M, Milani G (2019) Damage assessment and collapse investigation of three historical masonry palaces under seismic actions. Eng Fail Anal 98:10–37. https://doi.org/10.1016/j.engfailanal.2019.01.066
- Vanin F, Penna A, Beyer K (2020) A three-dimensional macroelement for modelling the in-plane and outof-plane response of masonry walls. Earthq Engng Struct Dyn 49:1365–1387. https://doi.org/10.1002 /eqe.3277
- Whitman RV, Reed JW, Hong ST (1973) Earthquake damage probability matrices. In Proceedings of the Fifth World conference on earthquake engineering. vol. 2. Rome, Italy, 2537–2540
- Yang L, Shami A (2020) On hyperparameter optimization of machine learning algorithms: Theory and practice. Neurocomputing 415:295–316. https://doi.org/10.1016/j.neucom.2020.07.061
- Zhao JX (2006) Attenuation relations of strong ground motion in Japan using site classification based on predominant period. Bull Seismol Soc Am 96:898–913. https://doi.org/10.1785/0120050122

Publisher's Note Springer Nature remains neutral with regard to jurisdictional claims in published maps and institutional affiliations.

Authors and Affiliations

Juan Pablo Muñoz Gálvez¹ D· Dina D'Ayala² D· Nuria Chiara Palazzi^{1,3} D· Juan Carlos de la Llera^{1,4} D

> Juan Pablo Muñoz Gálvez jpmunoz4@uc.cl

Nuria Chiara Palazzi nuria.palazzi@unab.cl

Juan Carlos de la Llera ¡cllera@uc.cl

- Research Center for Integrated Disaster Risk Management (CIGIDEN), ANID/FONDAP/1523A0009, Santiago, Chile
- UNESCO Chair in Disaster Risk Reduction and Resilience Engineering, University College London, England, UK
- Faculty of Architecture, Art, Design and Communications, Universidad Andrés Bello, Santiago, Chile
- Department of Structural and Geotechnical Engineering, Pontificia Universidad Católica de Chile, Santiago, Chile

